POST-SHOCK TEMPERATURES IN MINERALS

by

Susan A. Raikes*

and

Thomas J. Ahrens

Seismological Laboratory
Division of Geological and Planetary Sciences
California Institute of Technology
Pasadena, California 91125

*Present address: Geophysikalisches Institut
Universität Karlsruhe
Hertzstrasse 16, Bau 42
7500 Karlsruhe-West (21)
W. Germany

Abstract

An experimental technique has been developed for the measurement of post-shock temperatures in a wide variety of materials, including those of geophysical interest such as silicates. The technique uses an infra-red radiation detector to determine the brightness temperature of samples shocked to pressures in the range 5 to ∿30 GPa; in these experiments measurements have been made in two wavelength ranges (4.5 to 5.75μ; 7 to 14μ). Reproducible results, with the temperatures in the two wavelength bands generally in excellent agreement, have been obtained for aluminium-2024 (10.5 to 33 GPa; 125 to 260°C), stainless steel-304 (11.5 to 50 GPa; 80 to 350°C), crystalline quartz (5.0 to 21.5 GPa; 80 to 250°C), forsterite (7.5 to 28.0 GPa; ∿30 to 160°C) and Bamble bronzite (6.0 to 26.0 GPa; ∿30 to 225°C).

These results are generally much higher at low pressures (where they may even be in excess of the calculated shock temperatures) than the values calculated assuming a hydrodynamic rheology and isentropic release parallel to the Hugoniot but tend towards them at higher pressures. In aluminium-2024, the theoretical post-shock temperatures, assuming a fluid-like rheology, are 35 to 218°C, for the pressure range 10.5 to 33 GPa. However, the results are in considerably better agreement with values calculated assuming elasto-plastic behaviour (80 to 270°C) which probably also causes the high measured temperatures for stainless steel. In forsterite the measured values ranged from 65°C to 9.6 GPa (there was no detectable rise at 7.5 GPa) to 156° at 28.0 GPa, whereas the "hydrodynamic values" were 30 to 120°C. Values obtained for quartz were in excellent agreement with those calculated by Mashimo et al. (1979) using release adiabat data. It is concluded

that release adiabat data should be used, wherever available, for calculations of residual temperature, and that adequate descriptions of the shock and release processes in minerals need to be more complex than generally assumed.

Introduction

Shock wave equation of state data have long been used in the interpretation of impact metamorphism (e.g., Stöffler, 1971, 1972) and of density depth profiles of the earth obtained from seismic data (e.g., Al'tschuler, 1965). However, one of the limitations to these uses of Hugoniot data is the uncertainty in the temperatures reached both during the passage of the shock wave through the material and after unloading.

Shock temperatures have previously been calculated using Hugoniot data and the Mie-Grüneisen theory (e.g., Walsh and Christian, 1955; Wackerle, 1962; Ahrens et al., 1969, McQueen et al., 1970) which should yield reliable results for metals provided the rheology corresponds to fluid-like behaviour. However, the Mie-Grüneisen theory, when the material is treated as a single phase, is inadequate over much of the pressure range for which shock wave data exist for silicates, since these all undergo major phase changes which may involve substantial changes in thermodynamic properties and internal energy. Calculated Hugoniot temperatures can then be used as a starting point to obtain post-shock temperatures assuming isentropic release. Unfortunately, there are few cases where there are sufficient data to either experimentally determine or theoretically calculate isentropic release paths; moreover the assumption of isentropic unloading from shock states has never been explicitly verified

experimentally. Consequently, even if the Hugoniot temperatures were calculated correctly, large uncertainties could still exist in residual temperatures.

Calculations of post-shock temperatures in silicates, assuming release along isentropes lying above the Hugoniot (Fig. 1), with the release volume greater than the initial volume, lead to values that appear too low to account for some of the effects seen in recovery experiments (eg. Gibbons, 1974). Where release adiabat data exist for silicates, they have been used in the calculation of post-shock temperatures (eg. Gibbons and Ahrens, 1971; Ahrens and O'Keefe, 1972). This always leads to much higher, and possibly more credible, release temperatures (as is shown by the comparison in Table 1) largely because the release paths lie below the Hugoniot.

Early experiments to measure post-shock temperatures were limited to metals; using a photo-multiplier tube Taylor (1963) found values for copper shocked to pressures in the range 90 to 170 GPa that were in good agreement with those calculated by McQueen and Marsh (1970) using Mie-Grüneisen theory and fluid rheology, although later work by King et al., (1967) and Von Holle and Trimble (1976) using infra-red radiation detectors revealed considerable discrepancies between observed and calculated temperatures for copper shocked to pressures below 80 GPa. However, no attempts were made to extend this type of experiment to non-metals, largely because the supposedly lower temperatures, coupled with the low sensitivity of available detectors, meant that experiments such as those of King et al. were not feasible. Recent improvements in detector technology have now made it possible to design a system capable of measuring post-shock temperatures in silicates; the availability of such data should help resolve the current uncertainties.

Experimental Technique

Initial experiments were designed with the aim of investigating residual temperatures in silicates of geophysical interest shocked to pressures up to 30 GPa. The materials chosen were natural crystal quartz (cut perpendicular to the c axis) Bamble bronzite (from Bamble, Norway), which consists of large natural single crystals closely described by the formula $(Mg_{0.86}Fe_{0.14})SiO_3$ which have a porosity of 1 to 3%, and synthetic crystal forsterite (cut perpendicular to the c-axis). For completeness, the materials used as driver plates in the experiments, namely aluminium-2024 and stainless steel-304, were also studied.

The method developed involves the monitoring of radiation from the back (free) surface of a shocked sample with an infra-red radiation detector whose output may then be used to determine the brightness temperature of the sample. Since the residual temperatures for the pressure range to be investigated were expected to be of the order of 400°K, and the Planck distribution law gives a maximum in spectral radiance between 3 and 9 μ for black bodies radiating at temperatures from 1000 to 300°K (Touloukian and DeWitt, 1972) infra-red detectors were a logical choice for this study. In addition, since silicates behave as fairly good black bodies in the infra-red beyond ∿5μ, with the exception of a minimum in emissivity at ∿9μ (Lyon, 1965), the radiative output of the sample is also maximised. A schematic plan of the experimental configuration is shown in Fig. 2.

a) Production of the shocked state.

In these experiments, the shocked state was produced in the sample by the impact of a gun launched flyer plate. The technique is described in detail by Gibbons (1974) and Raikes (1978) and has been used by a

number of authors (eg. Ahrens et al., 1971; Ahrens and Gaffney, 1971; King and Ahrens, 1976). The velocity of the projectile is determined from the interval between obscurations (by the front of the projectile) of the two laser beams (Fig. 2); typical uncertainties in velocity are ±0.05 km/s. The shock pressure in the sample is then calculated using the impedance match method (eg. Duvall and Fowles, 1963) and the known Hugoniots of flyer plate, driver plate and sample materials. Estimates of the uncertainty in pressure determination, based on the accuracy of velocity measurement and scatter of the Hugoniot points, are ±0.5 to 1.0 GPa in the silicates.

After passing through the mylar window sealing the end of the barrel, the projectile makes contact across a shorting target made from thin copper foil and having a negligible effect on the projectile velocity, and finally impacts the target assembly, (Fig. 2). In order to achieve nearly one-dimensional planar flow upon impact of the projectile with the target, the target is carefully aligned using the normal reflection from the target surface of a laser beam shining down the centre of the barrel. The target assembly consists of a driver plate (1.5mm aluminium-2024 or stainless steel-304), followed by a 3mm thick silicate sample, 15mm in diameter; in the case of shots on metals the driver plate, now 3mm thick, is the sample.

b. Temperature measurement

The brightness temperature of the back (free) surface of the sample is determined from the output from an infra-red detector. This detector is mounted above the impact chamber (Figure 2), and monitors the back face of the sample via a mirror and optical system. The latter ensures that only the centre (~0.8 cm dia) of the sample is viewed, reducing the

contribution from radial release waves (also somewhat lessened by using a circular sample) and increases the efficiency of the detection system. The detector is connected via an amplifier to two oscilloscopes. One is triggered by the passage of the projectile past the first laser beam of the timing system, and records the detector output at a rate of 50 μs/div. This provides a back-up record in case of failure of the higher time-resolution recording, and a means of checking that no temperature signals are generated prior to the passage of the shock wave through the sample assembly. (Note that it also provides another means of determining the projectile velocity.) The second ocilloscope is triggered by the contact of the flyer plate with the shorting target, which is approximately 15 mm in front of the driver plate, just prior to impact; this writes at 5 μs/div, and it is the primary record that is used in temperature determination. The interpretation of this record is based on the assumption that the oscilloscope sweep is triggered at the moment of contact of the flyer plate with the shorting target; this was checked by analysing the timing of signals seen on the back-up record (50 μs/div) and by using a delayed trigger on the oscilloscope, and appears valid to within ±0.5 μs, which is close to the rise time of the systems. A typical record (such as that for bronzite at 15.5 GPa, Fig. 8c) shows a sharp rise in signal level as the shock wave arrives at the free surface of the sample followed by a level portion corresponding to the residual temperature, and then a subsequent rise due to air shocks generated at the end of the sample chamber and the destruction of the mirror. At high pressures, especially for metals which have a second peak in the record (Fig. 7), the level portion may not be clearly visible; in this case the post-shock temperature is determined from the signal

0.5 μs (InSb) or 0.75 μs (HgCdTe) after the free surface arrival. (These values are the rise times of the detection systems.) Problems in resolving the residual temperature were also encountered for quartz where an initial flash (Fig. 8a) made identification of the level portion uncertain at the highest pressures.

The InSb and HgCdTe detectors were operated at 77°K. They are enclosed in dewars cooled by liquid nitrogen; both were obtained from the Santa Barbara Research Centre (Goleta, California) and typical response curves, obtained from S.B.R.C., are shown in Fig. 3. Additional operational details are listed in Appendix A. A filter was used to limit the bandwidth of the InSb detector to 4.5 to 5.75μ in order to minimise the possibility of radiation from the metal driver plate, or metal-sample interface, being transmitted through the sample and causing errors in the temperature determination. (As can be seen from the transmission scans of Fig. 4, which were obtained using a Perkin-Elmer Model 180 Infra-red Spectro-photometer in a manner analogous to that described in Burns (1970), this is unlikely to be a problem for quartz or bronzite but the forsterite does transmit significantly up to 5μ.)

The InSb detector was used with a variable gain amplifier (Raikes, 1978); the system rise time, which is essentially limited to $\sim$0.2 μs by the chip itself, was $\lesssim$0.5 μs depending on the gain setting used. Although the HgCdTe is a faster material ($\lesssim$0.1μs), the rise time of the detector-amplifier system was $\lesssim$0.8μs because an electronic filter with a high frequency cut-off of 5MHz had to be used to reduce the large amount of high frequency noise which would otherwise have made accurate measurement of temperature impossible.

In order to convert the voltage record into a brightness temperature, the detector must be calibrated. This is best performed by heating the sample *in situ* to a known temperature, and recording the corresponding voltage output of the detector-amplifier system. This is easily done for metals, but would be very hard for the non-metals studied since they are extremely brittle and hard to heat in the experimental configuration without cracking. Instead, initial estimates of temperature were based on the assumption that the silicates behaved as black bodies using a calibration curve obtained for a "black" body, graphite. For quartz in range 5 to 8μ this is a reasonable approximation since the emissivity is greater than 0.9 (Touloukian and DeWitt, 1972), and is probably justified for the Bamble bronzite in the InSb range, since it does not transmit. However, the forsterite has a 20% transmittance at 4.5μ (dropping rapidly to less than 5% at 5μ), and all the silicates studied have a large drop in emissivity at around 9μ. This is clearly visible in the comparison of black body and quartz emittance spectra at temperatures from 250 to 500°K presented by Lyon (1965). Corrections for sample emissivity were determined using available data, which are unfortunately, largely for powdered minerals or rocks. The values of the emissivity for quartz and dunite (primarily forsterite) given by Buettner and Kern (1965), Lyon (1965) and Touloukian and DeWitt (1972) were used to calculate correction factors as follows:

The detector output S for an operating wavelength range from γ_1 to $\gamma_2\mu$ may be expressed as

$$S = \int_{\lambda_1}^{\lambda_2} E(\lambda,T)D(\lambda)P(\lambda,T)d\lambda \qquad (1)$$

where $E(\lambda,T) = E(\lambda)$ = emissivity (assumed independent of T)

$D(\lambda)$ = detector response, $P(\lambda,T)$ = Planck's function

λ = wavelength, T = absolute temperature

This may be integrated numerically and used to derive the ratio of the signal obtained for a silicate at temperature T to that for a black body at the same temperature. The correction factors are listed in Table 2 the values for bronzite were estimated from those for quartz and dunite based on a comparison of absorption spectra of the three materials.

Since the post-shock temperatures are measured after the interaction of the shock-wave with the free surface, and that interaction will cause roughening of the surface, a correction factor derived for a rough surface might be more appropriate; however, the values listed in Table 2 for polished surfaces will be used since these should yield an upper bound on the temperature. Two additional factors should be taken into account: one is that the absorption peak may shift during shock compression (e.g., Goto et al., 1979), and broadening of the absorption bands for SiO_2 has been observed in samples recovered after shock compression to pressures up to 52 GPa (Mashimo et al., 1979; Stöffler, 1974). The second is the possibility of triboluminescence, or some other form of non-equilibrium radiation such as might be associated with a phase change; in these cases the emissivity may even exceed unity. Because of these uncertainties, the black body temperatures may well be more reasonable estimates of the residual values and will be used later in a comparison of observed and calculated temperatures; the corrected values probably represent upper bounds to the post-shock temperatures.

Typical calibration curves are plotted in Figs. 5 and 6, and Table 3 gives the power law fits to the curves. Both detectors gave

extremely reproducible calibration curves, as is demonstrated by the two sets of points for aluminium in the case of InSb (these were obtained several weeks apart with a number of shots fired in between).

Sources of error.

Errors in temperature measurement can basically arise from two causes — those related to the sample, and those originating from outside sources. Prime among the latter is contamination of the signal by radiation from air shocks which can be of extremely high temperature. Owing to the geometry of the apparatus these should not be important prior to the arrival of the shock wave at the free surface of the sample, and, indeed, no earlier signal rises were detected. The only air shock likely to affect the post-shock temperature measurement would be one generated at the back of the sample itself, which should be eliminated by the sample vacuum chamber that is pumped down to $\lesssim$5m Torr ($\lesssim$0.7 Pa). To reduce further possible radiation from residual gases within this chamber heated by compression due to the shock wave, the chamber was flushed out with helium prior to each shot. Radiation from later air shocks, such as that generated at the end of the sample chamber as the window breaks due to the shock wave travelling down the chamber walls and impact of ejecta from the samples, is clearly visible on each record, and ultimately causes the detection system to saturate. If the samples were transparent, then radiation from the metal driver plate could add to the signal, but the rise should then precede the free surface arrival of the shock wave, and this does not appear to be the case. Anyway, the emissivity of the metal is substantially lower than that of the sample, so this effect should be relatively small, and both detectors were chosen to operate at wavelengths where the samples are

nearly opaque. (Forsterite does have a 20% transmittance at 4.5μ dropping rapidly to less than 5% at 5μ, and so may show minor effects due to transmitted radiation for the InSb detector.) Both the driver plate and the sample surface in contact with it were polished prior to mounting of the sample in order to minimise the "porous" surface interactions that could give rise to considerable heating (see e.g., Urtiew and Grover, 1974); this also reduces the likelihood of air being trapped in this interface, but this should be removed by the evacuation of the sample chamber. In order for the signal to be contaminated by radiation from the metal or the driver-sample interface, large changes must take place in the transmissivity of the sample under shock conditions; although changes have been reported in sapphire (Urtiew, 1974), these were decreases and at much higher pressures. It seems that this is not a likely source of error. Vibration of the detector-amplifier system could conceivably affect the output. However, the detection system was physically clamped in isolation from the gun, and vibrational effects were not apparent except for some HgCdTe shots where a negative signal of short duration (∿10 μs), obviously non-thermal in origin, was observed prior to impact with the shorting target, but the output returned to the zero level before the free surface arrival.

Two main sources of errors associated with the sample behaviour under shock are changes in emissivity and the effects of non-uniform heating. The former may be investigated by comparing the brightness temperatures obtained at different wavelengths, since the change would probably not be constant as a function of wavelength. Changes in emissivity may be related to phase changes, changes in surface properties and triboluminescence. In a recent work on residual temperatures in copper, Von Holle and Trimble

(1976) determined temperatures by using the ratio of detector signals obtained at different wavelengths. They believed this would reduce the likelihood of error due to changes in emissivity and the effects of surface processes, and yield a relatively unbiassed estimate of the post-shock temperature. Unfortunately, the signal to noise ratio is low, as at low temperatures and especially for metals where the emissivity is low, small errors in the measurement of detector output can lead to large changes in the ratio of the signals from the two detectors and totally unreasonable temperatures. In these experiments the ratio technique did not prove useful, although for the higher pressure shots the calculated ratio temperatures were, in fact, in good agreement with the separate brightness temperatures.

The effects of non-uniform heating may be more severe; they were estimated by calculating the temperature that would be measured if 10% of the surface were 100 or 200°K hotter than the remaining 90%. For a 100° excess, the discrepancy between "measured" and mean temperatures is close to the accuracy of measurement, i.e $\sim\pm$10%. However, for a 200° excess the differences may reach $\sim$30° (with the measured temperature being an over-estimate), although such a temperature distribution seems rather unlikely because of the energy partition that would be required. Non-uniform shock heating has been clearly demonstrated in silicates where such features as adiabatic shear zones (e.g., Grady, 1977) deformational twin lamellae and localised production of glass (e.g., in bronzite, Gibbons, 1974) have been observed. This non-uniform heating is believed to contribute to the complete loss of strength once the Hugoniot elastic limit is exceeded. The effect of surface processes

such as jetting can also bias the temperature measurements; these will presumably be more important in metals where the optical depth is of the order of angstroms, than in silicates where it is microns. To reduce the likelihood of jetting, the sample surfaces were polished, but not to a high gloss as this would reduce the emissivity. Surface processes are probably more important in metals where the infra-red optical depths are $\sim 10^{-10}$m, than silicates where they are microns.

Observations

a. Stainless steel-304 and Aluminium-2024

Typical detector output records are shown in Fig. 7: these are for the InSb detector, but records obtained with the HgCdTe detector were essentially similar except for the longer rise time and the fact that the amplifier saturated prior to the peak T_2. The origin of this later peak is unclear: the temperature correlates well with pressure, shock and free surface velocities for both stainless steel and aluminium, the correlation curves for the two materials are distinct even if a common temperature calibration curve is used it appears to be a material property, rather than some effect common to all shots, such as the compression of residual gas within the sample chamber (it was not observed in shots on silicates at similar pressures) and may be related to localised heating on break up of the sample or to the action of radial release waves.

The temperatures determined are listed in Tables 4 and 5: agreement between the two wavelength ranges is good, with the difference not exceeding the estimated uncertainty in measurement. Also tabulated are the corresponding black body temperatures, which should place a lower bound on the residual temperatures; the values for aluminium are probably

too low, since the maximum reported emissivity for roughened oxidised aluminium-2024 is ∿0.4 (Touloukian and Ho, 1972) which would imply temperatures of 90° to 260°C.

b. Silicates

Typical records obtained using the InSb and HgCdTe detectors are shown in Figs. 8 and 9. Unlike quartz and bronzite, forsterite has very different records for the two wavelength ranges, probably because it transmits up to 20% in the InSb range; the InSb temperatures may thus be contaminated by radiation from the sample-driver interface. The records for quartz have a characteristic short duration 'flash' which is probably associated with triboluminescence, a phenomenon documented in quartz shocked to similar pressures by Nielson et al., (1961); the black-body temperatures corresponding to this peak are unlikely to be significant. Black body and corrected temperatures for the silicates studied are listed in Tables 6 to 8.

Comparison of Observed and Calculated Temperatures

a. Calculational techniques

The most widely used method of calculating shock, and hence post-shock, temperatures is probably that developed for metals by Walsh and Christian (1955) who derived a differential equation relating the shock temperature T_H to the volume on the Hugoniot V_H and material properties. This equation has the general solution

$$T_H(V_H) = T_o \exp\left(-\int_{V_0}^{V_H} b(v)\,dv\right) + \exp\left(-\int_{V_0}^{V_H} b(v)\,dv\right) \int_{V_0}^{V_H} \frac{f(v)}{C_v} \exp\left(\int_{V_0}^{v} b(v)dv\right) dv \qquad (2)$$

Here T_o and v_o are the initial temperature and volume, C_v the specific

heat at constant volume, $b = \frac{1}{C_v}\left(\frac{\partial P}{\partial T}\right)_v = \frac{\gamma}{v}$ where γ = Grüneisen's parameter and $f(v) = \frac{dp}{dv}\frac{(v_o - v)}{2} + \frac{P}{2}$ evaluated at pressure, volume, points (P,v), along the Hugoniot.

A common assumption is that γ has the form

$$\gamma = \gamma_o\left(\frac{v}{v_o}\right)^n$$

where $n \gtrsim 1$ if $n = 1$, then b is constant and (2) reduces to the form actually derived by Walsh and Christian. Equation (2) is reduced to a difference equation and solved iteratively along the Hugoniot for T_H.

The derivation of (2) is based on two main assumptions: firstly that an ordinary fluid type equation of state is valid, which ignores the effects of rigidity or elasto-plastic work, and secondly that thermodynamic equilibrium exists in states behind the shock front. In addition, it is strictly valid only where the shock state is reached by a single step and not in the two wave-region associated with the Hugoniot elastic limit or phase changes; it must thus be modified for application to silicates such as those studied here. In the case of quartz, Wackerle (1962) modified the approach of Walsh and Christian by calculating temperatures along an "equilibrium" Hugoniot obtained from a segmented linear fit to the plot of effective shock velocity U^* against effective particle velocity u*, where U^* and u* are given by

$$U^* = v_o(P_H/(v_o - v_H)]^{1/2} \tag{3}$$

$$u^* = [P_H(v_o - v_H)]^{1/2} \tag{4}$$

where v_H is the volume corresponding to a shock pressure P_H. (These represent the true velocities only at high enough pressures where

the two-wave structure is overdriven.) Such equilibrium Hugoniots may be defined for quartz anf forsterite using Wackerle's 1962 data for quartz and the single crystal datum reported in Appendix B, the data for polycrystalline forsterite (McQueen, 1968) and ∿490 porous polycrystalline forsterite (Ahrens et al., 1971). However, the data for bronzite are so scattered probably because of varying porosity, that no satisfactory equilibrium Hugoniot can be derived; instead, Walsh and Christian temperatures were calculated along Hugoniots derived from Birch Murnaghan adiabats using the constants of Table 9 and an initial specific volume of 0.304 cm^3/g (for details of this method see, e.g., Davies, 1974). A theoretical Hugoniot was also used in calculations involving forsterite.

An alternative approach was described in detail by Ahrens et al. (1969). The increase in internal energy ΔE_H of a material shocked to a state with volume v_H and pressure P_H is given by the Rankine-Hugoniot conservation equation increase in internal energy resulting from isothermal compression at T_o from an initial volume to a final volume v_H plus isovolumic heating to the shock temperature T_H. In this case

$$\Delta E_H = 1/2\ (P_H + P_O)\ (V_o - V_H) = \int_{V_O}^{V_H} \left(\frac{T\gamma C_v}{v} - P\right)_{T_o} dv + \frac{P_H - P_T}{b} \qquad (5)$$

where P_T is the pressure on the isotherm, at volume, V_H.

This is solved for P_T, and T_H determined from the expression for the pressure difference between the Hugoniot and the isotherm

$$P_H = P_T = b \int_{T_o}^{T_H} C_v\, dT \qquad (6)$$

where $b = \gamma/v$ is assumed constant.

This formulation is easily adapted for inclusion of the Hugoniot elastic limit, and for calculating shock temperatures in the high pressure regime for materials which undergo phase changes. Both quartz and bronzite do so in the pressure range investigated (starting at $\sim$ 15 GPa and $\sim$ 13.5 GPa respectively) but neither is complete until $\gtrsim$ 40 GPa. The highest pressure measurements here are thus in the mixed phase regime - in quartz at 20 GPa the phase change is $\lesssim$ 25% complete (Grady et al., 1974). Calculations in the mixed phase regime are extremely complicated, the Hugoniot state may be assumed to be a mixture of high and low pressure phases in thermal and mechanical equilibrium and equations derived which can be solved numerically for the mass fraction of transformed material and the Hugoniot temperature at a series of points on the mixed phase Hugoniot (Ahrens et al., 1969). However, in view of the uncertainties in the mechanism of the phase change, and in bronzite its nature (the high pressure phase is probably majorite (Smith and Mason, 1970), but may be ringwoodite plus stishovite (Ahrens and Gaffney, 1971)) and the pressure range studied, the effects of the phase change were ignored, except in so far as they changed the shape of the equilibrium Hugoniot for quartz. The calculation of post-shock temperatures in the mixed phase regime is further complicated by the behaviour of the high pressure phase on release, when it may transform to an amorphous form (Grady, et al., 1974).

The calculational methods derived by Walsh and Christian and Ahrens et al. both yield values for Hugoniot temperatures, and the residual temperatures must be determined from these. It is generally assumed that the release is isentropic, in which case the residual temperature T_R is

given by

$$T_R = T_H \exp\left\{ \int_{V_R}^{V_H} b(v)\ dv \right\} \qquad (7)$$

where V_R = volume on release, often assumed equal to V_o. For cases where the release path is known, the residual temperature may be calculated directly, as described by Gibbons (1974): the energy in the Hugoniot state is equated to the change in internal energy due to the rise in temperature from the initial value T_o to the residual value T_R plus the energy change on release. Thus

$$1/2\ (P_H + Po)\ (V_o - V_H) = \int_{V_H}^{V_R} [Pdv]_{release} + \int_{T_o}^{T_R} C_p\ dT \qquad (8)$$

where V_R is the volume on release and C_p the specific heat at constant pressure.

b. Results for Aluminium and Stainless Steel

Since the Walsh and Christian approach was developed specifically for application to metals (in the absence of phase changes) where the Hugoniot elastic limits are low ($\lesssim$1.0 GPa), the application of this technique should yield results in good agreement with the experimental observations. Fig. 10 (a) and (b) show the values of shock (dashed lines) and post-shock temperature (solid curves) calculated for stainless steel-304 and aluminium-2024 using this approach; they are the same as those given by McQueen et al., (1970). Also plotted are the observed values, and, as can be seen, there is practically no agreement. In fact, the measured residual temperatures are, at low pressures, in excess of the calculated Hugoniot temperatures. Discrepancies between observed and theoretical residual temperatures in metals have also been reported

by other workers (e.g., Von Holle and Trimble, 1976) using similar experimental techniques, and the question of the validity of the measurement arises. Certainly, the measured values may be too high because of surface processes or changes in emissivity -- though they are consistent in two wavelength ranges -- but the fact that they tend towards the theoretical values with increasing pressure suggests that the theory does not include some effect that dominates at low pressures. (Allowing for reasonable emissivity changes, the observed values are, in fact, still higher than those calculated.) The observed temperatures for steel may at first seem high when compared to the small amount of heating apparently observed in steel containers used in recovery experiments; however, these containers are not examined immediately, and the initial post-shock temperatures will quickly decay owing to thermal conduction. This is borne out by the observations of Schneider and Stilp (1977) who used thermocouples to measure the temperatures within large steel targets as a function of time and distance from the centre of impact by small steel cylinders and lead bullets. The time resolution of their measurements was only 50 ms, and they found that the temperature decayed rapidly as a function both of time and of distance away from the impact. Since in the current experiments the temperature at the centre of impact is observed within 1 μs of the shock wave arriving at the free surface, the high observed temperatures are not inconsistent with the maximum increase of 18°C observed 1.2 (or approximately the crater radius) cm from the impact centre by Schneider and Stilp.

One obvious omission from the Walsh and Christian formalism is the effect of elasto-plastic work. Although the metals have low Hugoniot elastic limits, they retain some rigidity after yielding, and may undergo

stress-hardening. The latter was reported by Fowles (1961), who demonstrated that an elasto-plastic equation of state should be used for aluminium shocked to pressures up to ∿15 GPa. This concept was developed in detail by Lee and Liu (1967) and Lee and Wierzbicki (1967) who developed a treatment allowing direct calculation of temperature along the Hugoniot curve which incorporates the effects of material strength and finite unisotropic strain. Foltz and Grace (1969) carried out the analysis for polycrystalline aluminium having a yield strength comparable to that for aluminium-2024; whilst their analysis may not be strictly valid for the alloy used in these experiments, a comparison of their values for Hugoniot temperature (the dash-dot line in Figure 10(b)) and the measured residual temperatures is interesting. As can be seen, their calculated values are considerably in excess of the Walsh and Christian values at low pressures, but converge with them at higher pressures, which is precisely the behaviour observed in the measured residual temperatures. Although the release path is not certain, it has been proposed that for metals the release from shock pressure P_H occurs in two stages: first an elastic release (isentropic) to a pressure $P_H - 2Y$, where Y is the Hugoniot elastic limit, followed by plastic release parallel to the Hugoniot (see e.g., Fowles, 1961; Al'tschuler, 1965). The post-shock temperatures indicated by the dotted curve in Figure 10(b) were derived from Foltz and Grace's Hugoniot temperatures assuming this form of release path with Y = 0.8 GPa. These values are in reasonable agreement with experimental observations (which may be slightly high due to changes in emissivity). Unfortunately, a similar calculation cannot be made for an alloy like stainless steel where the constants required are not

really defined. However, the relationship between the observed and Walsh and Christian values (Figure 10(a)) is similar to that observed for aluminium, and plastic deformation of the lattice has been observed in recovery experiments for pressures up to 50 GPa (e.g., Murr, 1975; Smith, 1958). The post-shock temperatures indicated by the solid line in Figure 10(a) were calculated from the Hugoniot temperatures assuming a simple isentropic release path; some allowance for elasto-plastic behaviour may be made by assuming a release path as indicated above and calculating the residual temperatures directly using 8. This yields the dotted line in Figure 10(a), but the agreement between experiment and theory is not substantially improved.

It is concluded that elasto-plastic work, which is not included in the Walsh and Christian formalism, causes significant heating at low pressures resulting in large differences between measured and calculated temperatures. However, at higher pressures ($\lesssim$30 GPa for aluminium, $\lesssim$50 GPa for stainless steel) the Walsh and Christian approach appears to predict values close to those measured experimentally.

c. Silicates

A comparison between the observed and calculated post-shock temperatures for quartz is presented in Fig. 11. The agreement between the observations and the residual temperatures calculated directly from release adiabat data by Mashimo et al. (1978) is very good, and this method of calculation is certainly to be preferred. However, the values calculated by Wackerle (1962) corrected for an initial temperature of 24°C are also remarkably close, to those observed except for the lowest and highest pressure points. The agreement may be improved by determining residual temperatures from the Hugoniot temperatures using

minimum release volumes estimated from the free surface and particle velocities given by Wackerle following the method described by Lyzenga and Ahrens (1978) or the release volumes given by Grady et al. (1974).

Temperatures calculated using the method of Ahrens et al. (1969) using values of 6 and 8 GPa for the Hugoniot elastic limit (the lower and upper bounds given by Wackerle for z-cut quartz) were much too low; the observed values are in fact greater than the calculated shock temperatures. Similar discrepancies were also noticeable for bronzite and forsterite, and may arise in the determination of the isotherm; it suggests this calculational technique is inadequate in the pressure range studied.

For bronzite, none of the existing calculational techniques produced adequate agreement between theoretical and observed post-shock temperatures (Fig. 12) and since the observed values are generally in excess of the calculated shock temperatures some process must occur which results in greater heating on compression. (This may be related to the effects of sample porosity: the apparent temperature drop between 20.7 and 25.0 GPa for InSb measurements probably reflects the fact that the latter sample had a lower density of fine cracks than usual.) Attempts were made to improve the Walsh and Christian calculations by using a temperature, as well as volume, dependent Debye temperature in calculating the specific C_v via the Debye model. However, the post-shock temperatures are relatively insensitive to these refinements and no marked improvement in agreement was produced. The calculations of residual temperature are also fairly insensitive to the behaviour of Grüneisen's parameter provided it is the same on compression and on release. A model in which the Grüneisen parameter is higher on compression than release yields higher residual temperatures. Although we cannot defend such a model in detail, this idea does in face have a good physical basis,

since the shock and release processes are certainly different. In particular, the observations of release paths lying beneath the Hugoniot (e.g., Fig. 1) and the apparent hysteresis in the shock and release process are not fully understood; they may be related to the behaviour of γ. A model in which $\gamma_o(=\gamma(V_o)$ was assumed to be 2.5 on compression and 1 on release produced somewhat better agreement, especially at high pressure, but a Grüneisens parameter of at least 3 during shock compression would be required to produce agreement at pressures less than 15 GPa. In this case the calculated release temperatures (assuming $\gamma_o = 1$) would be too high at pressures of ∿25 GPa, so a more complicated behaviour of γ would have to be postulated. This does not seem justified since the theoretical Hugoniot does not adequately describe the effects of varying sample porosity, and the high temperatures may be largely due to this; furthermore, the effect of the phase change has been neglected — although this would provide some justification for changing the behaviour of the effective γ at 15 GPa.

The results of the temperature calculations for forsterite are shown in Fig. 13; at this stage it should be noted that the 10 and 15 GPa measurements using the InSb detector are probably contaminated by radiation from the sample driver interface, as discussed previously. The observed temperatures are considerably in excess of the values calculated for the non-porous polycrystalline forsterite using the equilibrium Hugoniot (curves A, A', Fig. 13(a)), and are also greater than the values calculated for the theoretical Hugoniot (C, C') although there is some indication that the measurements tend towards the latter at high pressures. The values calculated for the "porous" equilibrium Hugoniot

(B, B') are much higher than the observations except for the doubtful InSb points; this is not surprising since the samples were only $\lesssim$1% porous, and not 4%. As with bronzite, a better fit to the observations may be obtained using the Walsh and Christian approach but assuming that γ_o is higher on compression than release; a fairly good fit resulted from using the theoretical Hugoniot with $\gamma_o = 2.5$ on compression and $\gamma_o = 1$ on release. However, although temperatures calculated by the conventional methods of Walsh and Christian and Ahrens et al. are much lower than the observations at low pressure, they converge at higher pressure, which is reminiscent of the behaviour observed in stainless steel and aluminium and ascribed to elasto-plastic effects. A detailed investigation of the process of dynamic yielding in forsterite would indicate whether such effects were possible here; if the behaviour of forsterite is indeed similar to that of metals, then the release path may be approximated by the two stage elasto-plastic path that was described earlier and is sketched in Fig. 14. In this case an estimate of the release temperature may be obtained by calculating the energy difference between the shock and release paths (the shaded area in Fig. 14) and equating it to the increase in internal energy as in equation 8. This results in the temperatures shown by the heavy line in Fig. 13(b); the agreement between these values and the observations is good at $\sim$10 GPa, but large differences exist at higher pressures, as would be expected if the material underwent a gradual loss of strength that was complete by $\sim$25 GPa. (Experimental evidence indicates that the loss of strength is in fact complete by $\sim$20 GPa; see Appendix B.) This calculation ignored the fraction of energy going into permanent deformation of the lattice, which may be estimated as follows: the free energy of

a crystal is increased by about $\mu b^3/2$ per atomic length of dislocation, where μ is the shear modulus and b is the average length of the Burgers vectors of the crystals. With $b \sim 5\text{Å}$, $\mu = 80$ GPa, and a dislocation density of 10^{11} cm^{-2}, which is probably rather high for these pressures (R. Jeanloz, personal communication, 1978), allowing for the deformational energy results in a 15% or smaller reduction in the increase in thermal energy due to shock compression and release. This is equivalent to a 6°C (or smaller) decrease in release temperatures from the values plotted in Fig. 13(b).

Discussion

The experimental technique described here has proved useful for measuring post-shock (brightness) temperatures in a variety of metals and silicates. Initial experiments produced results which are, in general, consistent at two wavelength ranges (from 4.5 to 5.75μ and from 7 to 14μ) and for different samples of the same material shocked to similar pressures. Although the consistency of the results suggests that the measured temperatures are indeed representative of the residual temperatures in the shocked samples, uncertainties still exist in the precision of the metals because of the lack of information on the effect of surface process, which are likely to be important in metals, and changes in emissivity under shock conditions. In particular, little data is available on the emissivity of the silicates studied, even under normal conditions; and if such data were available more accurate correction factors could be estimated, although the possibilities of non-equilibrium radiation with an emissivity greater than unity and changes in emissivity under shock conditions would remain. Experimental investigation of the

latter, if possible, would be most valuable. One effect that may influence the measurements of residual temperatures in aluminium is the ejection of material from the surface; this has been studied by Asay et al. (1976) for pressures of ∿25 GPa and is quite significant. A further study by Asay (1977) showed that material ejection was highly dependent on the rise-time of the shock wave, so the effect of material ejection on temperature measurement might be investigated by determining residual temperatures for different shock rise-times.

Measured temperatures in quartz, which is known to undergo a complete loss of strength after the Hugoniot elastic limit is exceeded, were in good agreement with those calculated by Mashimo et al. (1978) from release adiabat data, and in reasonable agreement with those derived from the equilibrium Hugoniot of Wackerle (1962) using estimated release volumes. These calculations did not include the affects of the quartz to stishovite phase change which begins at ∿15 GPa; however there was only a slight change in the rate of increase of measured temperature with pressure in this region.

For both the metals studied, and for forsterite and bronzite, the measured temperatures were considerably in excess of those predicted using conventional fluid rheology assumptions, although the absence of release adiabat data for forsterite and bronzite meant that a comparison with temperatures calculated in the optimal manner (i.e. using equation 8) was not possible. In all these cases some process is required which leads to higher calculated shock temperatures, especially at low pressures, and less energy loss on release. For metals, this is probably elasto-plastic work, which dominates at low pressures: reasonable agreement was

found between the elasto-plastic calculations of Foltz and Grace (1969) and measurements for aluminium. An attempt was made to model such a process in bronzite and forsterite by allowing Grüneisen's parameter to be higher on compression than on release, and for forsterite reasonable agreement was obtained with $\gamma_o = 2.5$ on compression, $\gamma_o = 1$ on release (note that under standard conditions the thermodynamic Grüneisen's parameter is 1.17). No strict physical justification for postulating a different γ for shock compression from that on unloading is attempted here; however, this type of behaviour does provide better agreement between theory and observations although the model is somewhat non-unique. The differences between observed and predicted release adiabats and the hysteresis observed in shock unloading suggest that some change in material properties may occur prior to release from the shock state, and thus irreversible behaviour of the anharmonic properties is not incredible. Another possibility is that elasto-plastic work may also be important: although quartz has been observed to undergo a complete loss of material strength beyond the Hugoniot elastic limit, the same has not been demonstrated for forsterite. Calculations of residual temperatures in which it was assumed that forsterite behaved in an elasto-plastic manner similar to that proposed for metals yielded values that agreed well with observations at 10 GPa but were much higher at higher pressures. This suggests that forsterite undergoes a much more gradual loss of material strength beyond its elastic limit than does quartz, and that elasto-plastic effects may be important at pressures below $\sim$25 GPa.

Classifications of shock metamorphism such as that of Stöffer, (1971) are based on a detailed analysis of the physical characteristics

of the specimen (such as the amount of fracturing, undulatory extinction or presence of glass.) Estimates of the temperature range corresponding to each class of metamorphism have then been made using calculated values of the shock and post-shock temperatures: Stöffler used the values of Wackerle (1962) for quartz and Ahrens et al. (1969) for feldspars. The results of the present study indicate that the former are fairly reliable below ∿20 GPa (when corrected for the right initial temperature), but the calculational technique of Ahrens et al. yielded temperatures that were substantially lower than those observed, so that the values used by Stöffler for feldspars are also likely to be low. Indeed, observations of recovered shocked samples suggest that this is the case both in feldspars (e.g. Gibbons, 1974) and dunite (e.g. Reimold and Stöffler, 1978). Measurements of the electrical conductivity of shocked dunites (Schulein et al. 1978) show increases that are also more easily explained if the actual temperatures are higher than those calculated. The main implication of this study for impact metamorphism is that temperatures in forsterite and bronzite appear considerably higher than the theoretical values, especially for porous samples, and so the effects of impact metamorphism on basic rocks such as lunar basalt may differ from those expected on the basis of theory and lead to erroneous conclusions regarding the nature of the impact. Since the partitioning of energy during impact processes is important in calculating the thermal history of an accreting planet, residual temperature data such as those presented here could provide useful constraints on the temperature distribution during accretion.

One important assumption used in the temperature calculations was

that equilibrium existed behind the shock-front. Temperatures measured in these experiments were generally higher than those calculated, but other factors leading to errors in the calculation make it hard to assess the validity of this assumption. A systematic investigation of differences between shock effects seen in shock recovery experiments and in naturally shocked samples where the peak pressures are of longer duration could help clarify this point. Such differences certainly exist - for example, the substantial amount of coesite observed in natural, but not shock-recovery, specimens (Stöffler, 1972) and might yield important information on the nature of equilibrium in shock processes.

It has been emphasised that the release path is of critical importance to the determination of post-shock temperatures, yet it has generally been assumed that the release is isentropic; if this is not the case, then discrepancies between measurement and theory are not surprising. Recently Kieffer and Delany (1979) have placed new and useful constraints on the assumptions of isentropic flow in solids under decompression. Viscous heating on release would lead to higher residual temperatures.

Release adiabats which lie below the Hugoniot (see Fig. 1) lead to higher residual temperatures in better agreement with the observations, yet it seems strange that if the material is essentially unchanged by shock compression and release, it should occupy a smaller volume on release when it is hotter than it was initially. Measurements of the parameters on release adiabats are often made at relatively high pressures

($P_H > P_R >> 0$, where P_H is the shock pressure and P_R the point at which release measurements are made) and so yield information on the initial slope of the release adiabat which may then be extrapolated to yield the release volume. Such an extrapolation is illustrated schematically in Fig. 15 by the dashed line: this yields a release volume smaller than v_0; however the actual path may be as shown by the dotted line. Since the area between the Hugoniot and the two release curves is the same, they will give the same residual temperatures if (8) is used. Assuming that the material is unchanged, then the release volume may be estimated from the post-shock temperature and the mean thermal expansion coefficient $\bar{\alpha}_p$, and can provide additional constraints on the release path. Table 10 lists the estimated release volumes for the materials studied: in fact, for the silicates and stainless steel they are not very different from the initial volumes.

It was hoped that this study would yield some definite information on the behaviour of Grüneisen's parameter, which is critical for the reduction of shock wave data to the form needed for comparison with density-depth profiles within the earth. However, post shock temperatures are not very sensitive to the behaviour of γ (unless it is different on shock compression and release) and appear more greatly influenced by the release path, in particular the release volume. There seems to be no need to postulate unusual behaviour of γ for quartz to $\sim$25 GPa, although the high observed values of residual temperatures in forsterite and bronzite suggest that present rheological models used in shock temperature calculations, at least below $\sim$25 GPa, are either inadequate, or the effective Grüneisen parameter is high ($\gamma_o \sim 2.5$) on compression and decreases to near its zero pressure value ($\gamma_o \sim 1$) upon adiabatic release.

Acknowledgements

The authors thank Raymond Jeanloz and Gregory Lyzenga for many interesting and stimulating discussions; they are also indebted to Wayne Miller and Victor Nenow, who designed and built the variable gain amplifier used with the InSb detector, and to the staff of the Santa Barbara Research Centre, Goleta, California for their advice concerning detector operation. We thank D. Stöffler for both his comments on impact metamorphism, and the final version of the manuscript. This work was supported by NASA under grant NGL 05-002-105. Contribution No. 3143, Division of Geological and Planetary Sciences, California Institute of Technology, Pasadena, California 91125.

Table 1

CALCULATED POST SHOCK TEMPERATURES
IN FUSED QUARTZ AND OLIGOCLASE,

using the Mie-Grüneisen Theory (A) or Release Adiabat Data (B)

Shock Pressure GPa	Post Shock Temperatures, °C			
	Fused Quartz		Oligoclase	
	A[1]	B[2]	A[3]	B[4]
10.0	0	80		
15.0	0	450		
18.0			27 - 35	269-386
25.0	0	1220		
27.2			129-206	> 742
30.0	470	1480		
40.0	1860	2180		
41.7			327-395	>1031
50.0	3310	2820		

1. Wackerle (1962)
2. Gibbons and Ahrens (1971)
3. Ahrens et al. (1969)
4. Ahrens and O'Keefe (1972)

Table 2

ESTIMATED SIGNAL CORRECTION FACTORS

$$\text{Correction factor} = \frac{\text{Silicate signal}}{\text{Black Body signal}} \quad \text{(values to nearest 0.05)}$$

	T = 400°K		T = 600°K	
	InSb	HgCdTe	InSb	HgCdTe
Quartz (polished)	0.90	0.80	0.85	0.80
Quartz (rough)		0.90		0.90
SiO_2	0.90		0.90	
Dunite (polished)	0.85	0.90	0.80	0.90
(Bronzite	0.9	0.85	0.9	0.85)

Table 3

POWER LAW FITS TO CALIBRATION CURVES

$S = a(T-24)^b \times 10^{-5}$; coefficient of determination r^2

	Black Body			Stainless Steel			Aluminium-2024		
	a	b	r^2	a	b	r^2	a	b	r^2
InSb	7.21	1.87	.99	2.21	1.93	.98	3.08	1.71	.95
HgCdTe	10.9	1.45	.97	10.05	1.32	.97	2.68	1.43	.98

Table 4

MEASURED POST-SHOCK TEMPERATURES

IN STAINLESS STEEL-304

Temperature, °C

	InSb		HgCdTe		Peak
Pressure, GPa	SS	BB	SS	BB	(InSb)
11.5			80	60	
11.7	110	75			250
13.0	125	80			600
14.5			130	85	
16.0	145	100	145	95	830
23.0	195	130			1530
24.2			200	130	
43.0	325	230			
50.0	355	250			1820

SS = calibration using stainless steel

BB = black body temperature

Uncertainties in temperature: ±15° below 150°, ±10° above 150°.

T_o = 24°C

Table 5

MEASURED POST-SHOCK TEMPERATURES

IN ALUMINIUM-2024

Temperature, °C

Pressure, GPa	InSb		HgCdTe		Peak (InSb)
	AL	BB	AL	BB	
10.5	125	50			
11.5			140	65	
12.5	135	55			1250
15.0	150	60			
15.7			155	70	
18.5	175	75	185	80	1430
25.0			220	90	
27.0	230	105			2200
32.5	250	120			
33.0	260	127			3800

AL = calibration with aluminium

BB = equivalent black body temperature

Estimated uncertainties: ±20°C below 200°C, ±10°C above 200°C

T_o = 24°C

Table 6

MEASURED POST-SHOCK TEMPERATURES IN QUARTZ

Temperature, °C

	InSb			HgCdTe		
Pressure, GPa	Flash	BB	Corr.	Flash	BB	Corr.
5.0	235	80	87			
5.5				110	75	85
8.0	180	100	105			
9.5	225	120	125	320	115	127
10.8	245	155	162			
11.5	252	160	170			
15.0	340	177	187			
15.5*				—	160	180
17.5	377	185	195			
19.5				706	320	340
20.0	390	242	255			
21.5	425	250	265			

*This was a very faint record, and may not be reliable.

Uncertainties: ±10°C below 100°C, ±5°C above 100°C

T_o = 24°C

Table 7

MEASURED POST-SHOCK TEMPERATURES IN FORSTERITE

Temperature, °C

	InSb			HgCdTe	
Pressure, GPa	Flash	BB	Corr.	BB	Corr.
7.5	180	<50°	(no detectable rise)		
9.6*	237	105	115	65	77
15.0**	260	136	145		
18.0				105	112
20.2	285	140	152		
21.0				120	125
24.0				160	165
24.5	270	148	160		
28.0	300	156	167		

*Two peaks (175, 237°C); residual temperature corresponds to the difference between the levels after the second and first peaks.

**Two peaks (135, 260°C); residual temperature estimated as before.

Estimated uncertainties: ±10°C below 100°C, ±5°C above 100°C

T_o = 24°C

Table 8

MEASURED POST-SHOCK TEMPERATURES IN BAMBLE BRONZITE

Temperature, °C

Pressure, GPa	Peak	BB	Corr.	BB	Corr.
6.0		$\lesssim$ 50° (no detectable rise)			
10.3	123	100	105		
11.0				110	120
14.8				145	160
15.5	185	147	157		
20.7	225	200	213		
21.5				185	200
25.0	200	175	185		
26.0				225	240

Uncertainties: ±10°C below 100°C, ±5°C above 100°C

T_o = 24°C

Table 9

SOME CONSTANTS RELEVANT TO THE CALCULATION

OF TEMPERATURES IN SHOCKED SILICATES

	ρ_o^{-1} cm^3/gm	γ_o	Θ_D[1] °K	$\bar{m}$	K_{os} GPa	K'_{os}
Quartz	.377	.703[2]	1050	20.03	37.7[2]	6.4[2]
Forsterite	.310	1.17[2,3]	900	20.12	126.7[3] / 128.8[4]	5.37[3]
Bronzite	.298[5]	.907	950	20.96	103.5[5]	9.59[5]
	.307	1.56[5]			105.0[7]	5.3[6]

γ_o = thermodynamic Grüneisen parameter

Θ_D = Debye temperature

$\bar{m}$ = mean atomic weight

K_{os} = zero pressure adiabatic bulk modulus

$$K'_{os} = \left(\frac{\partial K_{os}}{\partial P}\right)_T$$

1. Debye temperatures derived from fitting specific heat data from J.A.N.A.F. Tables.
2. Values from Anderson et al. (1968)
3. Kumazawa and Anderson (1969)
4. Graham and Barsch (1969)
5. Frisillo and Barsch (1971) $[Mg_{0.8}Fe_{0.2})SiO_3]$
6. Chung (1971); preferred value yielding better fit to Hugoniot data.
7. Kumazawa (1969)

Note: $\frac{\gamma}{V}$ was generally assumed constant.

Table 10

ESTIMATED RELEASE VOLUMES

	Al-2024	SS-304	Quartz	Forsterite	Bronzite
v_o (cm^3/g)	0.359	0.127	0.377	0.310	0.302[+]
$\bar{\alpha}_p$	8×10^{-5}	5×10^{-5}	3.5×10^{-5}	2.6×10^{-5}	2.4×10^{-5}
Pressure, GPa					
5	--	--	0.3776	∿0.310[++]	∿0.302[++]
10	0.361	0.1274	0.3782	0.3104	0.3026
15	0.363	0.1276	0.3789	0.3105	0.3029
20	0.364	0.1279	0.3799	0.3107	0.3032
25	0.365	0.1281	--	0.3111	0.3031/ 0.3035

+ Theoretical zero-pressure density, (Ahrens & Gaffney, 1971)
Actual initial volume ∿0.304 cm^3/g

++ No detectable temperature change

References:

Ahrens, T. J., D. L. Anderson and A. E. Ringwood, Equations of state and crystal structures of high-pressure phases of shocked silicates and oxides, Rev. Geophys., 7, 667-707, 1969.

Ahrens, T. J. and E. S. Gaffney, Dynamic compression of enstatite, J. Geophys. Res., 76, 5504-5513, 1971

Ahrens, T. J., W. H. Gust and E. B. Royce, Material strength effect on the shock compression of alumina, J. Appl. Phys., 39, 4610-4616, 1968.

Ahrens, T. J., J. H. Lower and P. L. Lagus, Equation of state of forsterite, J. Geophys. Res., 76, 518-528, 1971.

Ahrens, T. J. and J. D. O'Keefe, Shock melting and vaporization of lunar rocks and minerals, The Moon, 4, 214-249, 1972.

Ahrens, T. J., J. D. O'Keefe and R. V. Gibbons, Shock compression of a recrystallized anorthositic rock from Apollo 15, Proc. Lunar Sci. Conf. 4th, 2575-2590, 1973.

Ahrens, T. J. and C. F. Petersen, Shock wave data and the study of the earth in The Application of Modern Physics to the Earth and Planetary Interiors, S. K. Runcorn, ed., 449-461, Wiley-Interscience, 1969.

Ahrens, T. J., C. F. Petersen and J. T. Rosenberg, Shock compression of feldspars, J. Geophys. Res., 74, 2727-2746, 1969.

Al'tschuler, L. V., Use of shock waves in high pressure physics, Sov. Phys. Usp., 8, 52-91, 1965 (English Trans.).

Anderson, O. L., E. Schreiber, R. C. Liebermann and N. Soga, Some elastic constant data on minerals relevant to geophysics, Rev. Geophys., 6, 491-524, 1968.

Asay, J. R. Effect of shock-wave rise time on material ejection from aluminium surfaces, Sandia Laboratories Report SAND77-0731, 1977.

Asay, J. R., L. P. Mix and F. C. Perry, Ejection of material from shocked surfaces, App. Phys. Lett., 29, 284-287, 1976.

Buettner, K. J. K. and C. D. Kern, The determination of infrared emissivities of terrestrial surfaces, J. Geophys. Res., 70, 1329-1337, 1965.

Burns, R. G., Mineralogical Applications of Crystal Field Theory, Ch. 4, pp. 49-77, Cambridge University Press, 1970.

Chung, D. H., Equations of state of pyroxenes in the (Mg, Fe)SiO_3 system, EOS Trans. Am. Geophys. U., 52, 919, 1971 (abstract).

Davies, G. F., Limits on the constitution of the lower mantle, Geophys. J. R. astr. Soc., 38, 479-503, 1974.

Duvall, G. E. and G. R. Fowles, Shock waves, Chapter 9, in High Pressure Physics and Chemistry, Volume II, R. S. Bradley, ed., Academic Press, London, 209-291, 1963.

Foltz, J. F. and F. I. Grace, Theoretical Hugoniot stress-temperature-strain states for aluminum and copper, J. Appl. Phys., 40, 4195-4199, 1969.

Fowles, G. R., Shock wave compression of hardened and annealed 2024 aluminum, J. Appl. Phys., 32, 1475-1487, 1961.

Fowles, G. R., Dynamic Compression of quartz, J. Geophys. Res., 72, 5729-5742, 1967.

Frisillo, A. L. and G. R. Barsch, Measurement of single-crystal elastic constants of bronzite as a function of pressure and temperature, J. Geophys. Res., 77, 6360-6384, 1972.

Gibbons, R. V., Experimental effects of high shock pressure on materials of geological and geophysical interest, Ph.D. Thesis, California Institute of Technology, 1974.

Gibbons, R. V. and T. J. Ahrens, Shock metamorphism of silicate glasses, J. Geophys. Res., 76, 5489-5498, 1971.

Goto, T., G. R. Rossman and T. J. Ahrens, Absorption spectroscopy in solids under shock compression, Proc. 6th AIRAPT International High Pressure Conference, Boulder, Colorado, 1979 (in press).

Grady, D. E., Processes occurring in shock wave compression of rocks and minerals, in High Pressure Research: Applications in Geophysics, M. H. Manghnani and Syun-Ibi Akimoto, eds., Academic Press, New York, 359-435, 1977.

Grady, D. E., W. J. Murri and G. R. Fowles, Quartz to stishovite: wave propagation in the mixed phase region, J. Geophys. Res., 79, 332-228, 1974.

Graham, E. K., Jr. and G. R. Barsch, Elastic constants of single-crystal forsterite as a function of temperature and pressure, J. Geophys. Res., 74, 5949-5960, 1967.

J.A.N.A.F. Thermochemical Tables, Nat. Stand. Ref. Data Ser., Nat. Bur. Stand. (U.S.), 37, 1141 pp., 1971.

Kieffer, S. W. and J. M. Delany, Isentropic decompression of fluids from crustal and mantle pressures, J. Geophys. Res., in press, 1979.

King, D. A., and T. J. Ahrens, Shock compression of ilmenite, J. Geophys. Res., 81, 931-935, 1976.

King, P. J., D. F. Cotgrove and P. M. B. Slate, Infra-red method of estimating the residual temperature of shocked metal plates, in Behaviour of Dense Media under High Dynamic Pressures, J. Berger, ed., Gordon and Breech, 513-520, 1968.

Kumazawa, M., The elastic constants of single-crystal orthopyroxene, J. Geophys. Res., 74, 5973-5980, 1969.

Kumazawa, M. and O. L. Anderson, Elastic moduli, pressure derivatives and temperature derivatives of single-crystal olivine and single-crystal forsterite, J. Geophys. Res., 74, 5961-5972, 1969.

Lee, E. H. and D. T. Liu, Finite-strain elastic-plastic theory with application to plane-wave analysis, J. Appl. Phys., 38, 19-27, 1967.

Lee, E. H. and T. Wierzbicki, Analysis of the propagation of plane elastic-plastic waves at finite strain, J. Appl. Mech., 34, 931-936, 1967.

Lyon, R. J. P., Analysis of rocks by spectral infrared emission (8 to 25 microns), Econ. Geol., 60, 715-736, 1965.

Lyzenga, G. A. and T. J. Ahrens, The relation between the shock-induced free surface velocity and the post-shock specific volume of solids, J. Appl. Phys., 49, 201-204, 1978.

Mashimo, T., K. Nishii, T. Soma, A. Sawaoka and S. Saito, Some physical properties of amorphous SiO_2 synthesized by shock compression of α-quartz, Submitted to Physics and Chemistry of Minerals, 1979.

McQueen, R. G., Shock wave data and equations of state, in Seismic Coupling, G. Simmons, ed., Advanced Research Projects Agency Meeting, 1968.

McQueen, R. G. and S. P. Marsh, Equations of state for nineteen metallic elements from shock-wave measurements to two megabars, J. Appl. Phys., 31, 1253-1269, 1960.

McQueen, R. G., S. P. Marsh, J. W. Taylor, J. N. Fritz and W. J. Carter, The equation of state of solids from shock wave studies, Chapter VII, in High-Velocity Impact Phenomena, R. Kinslow, ed., Academic Press, 293-417, 1970 (see also Appendix C, D, E, pp. 518-520, 521-529, 530-568).

Murr, Lawrence E., Interfacial Phenomena in Metals and Alloys, Addison Wesley, pp. 326, 348, 349, 1975.

Nielson, F. W., W. B. Benedick, W. P. Brooks, R. A. Graham and G. W. Anderson, Electrical and optical effects of shock waves in crystalline quarts, in Colloques Internationaux du Centre National de la Recherche Scientifique, No. 109, Les Ondes de Détonation, 391-414, 1961.

Raikes, S. A., Post-shock temperatures: their experimental determination, calculation and implications, Ph.D. Thesis Part II, California Institute of Technology, 1978.

Reimold, W.-V., and D. Stöffler, Experimental shock metamorphism of dunitic rocks, Lunar and Planetary Science IX, 955-957, Lunar and Planetary Institute, Houston, 1978.

Schneider, E. and A. Stilp, Measurement of temperature distributions within steel targets impacted by hypervelocity projectiles: method and preliminary results, Paper presented at the 7th International Congress on Instrumentation in Aerospace Simulation Facilities, RMCS, Shrivenham, England, September, 1977.

Schulien, S., V. Hornemann and D. Stöffler, Electrical conductivity of dunite during shock compression from 12.5 to 45 GPa, Geophys. Res. Lett., 5, 345-348, 1978.

Smith, C. S., Metallographic studies of metals after explosive shock, Trans. Metall. Soc. of AIME, 212, 574-589, 1958.

Smith, J. V. and B. Mason, Pyroxene-garnet transformation in Coorara meteorite, Science, 168, 832-833, 1970.

Stöffler, D., Progressive metamorphism and classification of shocked and brecciated crystalline rocks at impact craters, J. Geophys. Res., 76, 5541-5551, 1971.

Stöffler, D., Deformation and transformation of rock-forming minerals by natural and experimental shock processes. I. Behaviour of minerals under shock compression, Fortschr. Miner., 49, 50-113, 1972.

Stöffler, D., Deformation and transformation of rock-forming minerals by natural and experimental shock processes. II. Physical properties of shocked minerals, Fortschr, Miner., 51, 256-289, 1974.

Taylor, J. W., Residual temperatures in shocked copper, J. Appl. Phys., 34, 2727-2731, 1963.

Touloukian, Y. S. and D. P. DeWitt, Thermal radiative properties, non-metallic solids, T.P.R.C. Data Series, 8, Plenum Press, 1972.

Touloukian. Y. S., and C. Y. Ho, Thermal radiative properties of metallic elements and alloys, T.P.R.C. Data Series 7, Plenum Press, 1972.

Urtiew, P. A. and R. Grover, Radiation temperature in solids under shock loading, Fifth Symposium on Temperature, its Measurement and Control in Science and Industry, Nat. Bur. Stand., 4, 677-684, 1973, (Am. Inst. Phys.).

Urtiew, P. A., Effect of shock loading on transparency of sapphire crystals, J. Appl. Phys., 45, 3490-3493, 1974.

Urtiew, P. A. and R. Grover, Temperature deposition caused by shock interactions with material interfaces, J. Appl. Phys., 45, 140-145, 1974.

Van Holle, W. G. and J. J. Trible, Temperature measurement of shocked copper plates and shaped charge jets by two-colour IR radiometry, J. Appl. Phys., 47, 2391-2394, 1976.

Wackerle, J., Shock compression of quartz, J. Appl. Phys., 33, 922-937, 1962.

Walsh, J. M. and R. H. Christian, Equation of state of metals from shock wave measurements, Phys. Rev., 97, 1544-1556, 1955.

Appendix A Detector parameters.

Both detectors were purchased from the Santa Barbara Research Centre, Goleta, California.

a) InSb

The InSb detector used was a circular chip 1 mm in diameter having a detectivity of 5×10^{10} cm $Hz^{1/2}$/watt when operated at 77°K. It was operated with a fast matched pre-amplifier (S.B.R.C. Model A-230) consisting of a current mode operational amplifier with a feedback resistance of 1 kΩ and a non-inverting voltage mode post-amplifier; this stage had a gain of 500, and upper and lower 3db frequencies of 20 MHz and 1.35 kHz respectively. For use in measuring post-shock temperatures an additional amplifier with variable gain (from 1000 to 30,000) was used (Raikes, 1978). The minimum system rise time of ∿0.1μs is controlled by the detector chip itself. Sapphire windows were used with this detector.

b) HgCdTe

The chip used had an area of ? x 10^{-2} cm^2, a detectivity of 6.94×10^9 cm $Hz^{1/2}$/watt and a rise time of ∿ 100 nsec. It was used with a matched amplifier, S.B.R.C. Model A-120, having a gain of 1000. The amplifier consisted of an a-c coupled voltage mode amplifier plus a 499 Ω load resistor and circuitry to produce the bias current of 10 mA required by the detector; its upper and lower 3db frequencies were 10 MHz and 50 Hz respectively. The rise time of the detector-amplifier system is ∿ 0.05 μs; however, for operation at low signal levels it was found to produce an unacceptable level of very high frequency noise, and so had to be operated with a filter which raised the rise-time to ∿ 0.75μs. Barium fluoride or Irtran-2 (Kodak) windows were used with the HgCdTe detector.

Appendix B Dynamic Yielding in Forsterite

A detailed study of the dynamic yielding of single crystal forsterite has not been carried out. For the purpose of the present work a single measurement of the Hugoniot elastic limit along the c-axis of forsterite was undertaken in order to place some bounds on the rheological behaviour at relatively low shock stress.

Shock loading and recording were carried out with a modification of the 40 mm gun system described in Ahrens et al., 1971, 1973, although the optical recording was carried out using a Model 339B Beckman and Whitley continuous writing streak camera with a recently constructed xenon light source (described in Goto et al., 1978).

The sample, machined from the same aliquot as that utilised for the post-shock temperature measurements, was mounted on a 1.5 mm thick aluminium-2024 driver plate and impacted with a 4mm thick aluminium-2024 flyer plate. The pertinent measurements obtained in a single experiment (Figure B-1, Table B-1) provide a rather unequivocal measurement of the Hugoniot elastic limit amplitude, 8.68 ± 0.67 GPa, for a 3.7 mm thick sample. The velocity of the first shock, 8.72 km/s, is close to, but slightly higher than, the values of 8.543 km/s (Kumazawa and Anderson, 1969) or 8.564 km/s (Graham and Barsch, 1969) measured for the longitudinal velocity in the (3) direction. A similar relationship between the two velocities has been reported for quartz in various orientations (Wackerle, 1962; Fowles, 1967). The theoretical relation of the higher order elastic constants to the velocity of finite strength elastic waves, although reported for hexagonal symmetry (Fowles, 1967) has not been worked out for orthorhombic crystals.

The arrival time of the second shock, as indicated by the marked change in slope observed in the image of the inclined mirror (Figure B-1), can be interpreted in several ways depending on the rheology assumed for the sample material which has been compressed, and subsequently released, by the first shock (Wackerle, 1962). Our preferred analysis is simply to assume that the second shock velocity is given by

$$\overline{U}_2 = \frac{d + U_{1fs}\ (t_2-t_1)}{t_2-t_0} \qquad \text{B-1}$$

where d is the sample thickness, U_{1fs} the free surface velocity and (t_2-t_1) and (t_2-t_0) are the time interval between the arrival of the first and final shock and the travel time of the second shock to the free surface respectively (Ahrens et al., 1968). Equation B-1 ignores the interaction of the reflection of the first shock with the oncoming final shock front. The parameters of the final shock state (Table B-1) were obtained from an impedance match solution using the equation of state parameters given by McQueen et al. (1970) for aluminium-2024. Equation B-1 yields a final shock state which agrees well with the pressure-density trajectory calculated via the Murnaghan equation using parameters obtained from the ultrasonic data. If, on the other hand, the expression for the final shock velocity given by Ahrens et al. (1973), which assumes an elastic interaction of the reflected elastic shock with the oncoming final shock, is used a state with a greater compression is calculated (Figure B-2). Although the difference between the two solutions is not large, the calculation assuming no interaction, implying a loss of strength at pressures corresponding to the final shock state, appears to be definitely more consistent with the ultrasonic data. The relatively high Hugoniot elastic limit, followed by a (gradual) loss of shear strength, is consistent with the rheological behaviour inferred from the post-shock temperature measurements (Table 7).

Table B-1

Equation of State Data for Forsterite Shocked Along the (001) Direction (Shot 431)

Sample Mass	3.1546 ±0.0001g
Bulk Density	3.2158 ±0.005 gm/cm^3
Projectile Velocity	1.668 ±0.002 km/s

	First Shock State	Final Shock State
Shock velocity	8.717 ±0.068 km/s	6.554 ±0.067 km/s
Shock density	3.334 ±0.008 gm/cm^3	3.5716 ±0.0041 gm/cm^3
Shock pressure	8.68 ±0.67 GPa (Hugoniot elastic limit)	17.32 ±0.05 GPa
Free surface velocity	0.619 ±0.042 km/s	
Particle velocity		0.7246 ±0.0022 km/s

Figure Captions

Figure 1. Schematic diagram of Hugoniot and possible release adiabats. The solid release curves lie above the Hugoniot, and the dashed ones below it.

Figure 2. Schematic diagram of the experimental configuration. An oscilloscope recording the detector output at 50 μs/div is triggered by the passage of the projectile past the first laser beam. A record having greater time resolution (5 μs/div) is obtained from an oscilloscope triggered by the impact of the projectile with the shorting target.

Figure 3. (a) Response curve for InSb detector material.

(b) Response curve for HgCdTe detector material.

$D^*(\lambda,\nu)$ is the area independent sensitivity at frequency ν and wavelength λ.

Shaded areas indicate typical variations in detector sensitivity. (Details from the Santa Barbara Research Centre Catalogue)

Figure 4. Infra-red transmission scans for the silicate materials studied. The operating range of the filtered InSb detector and the start of the HgCdTe band are also shown.

Figure 5. Calibration curves for the InSb detector, operating in the wavelength range 4.5 to 5.75μ. The open and solid circles in the aluminium curve are the results of two different calibration runs.

Figure 6. Calibration curves for the HgCdTe detector.

Figure 7. InSb detector output records for aluminium and stainless steel. T_1 = residual temperature, T_2 = peak temperature, A = air shock.

Figure 8. InSb detector output records for the silicates studied. T_1 = flash temperature, T_2 (or T) = residual temperature. A = air shock.

Figure 9. HgCdTe detector output records for the silicates studied. T = residual temperature.

Figure 10. Comparison of observed and calculated temperatures in (a) stainless steel and (b) aluminium. The dashed curves are the Hugoniot temperatures calculated using the Walsh and Christian technique, and the solid curves the corresponding release temperatures. The dotted curve in (a) represents residual temperatures calculated directly assuming elasto-plastic release. The dot-dash and dotted curves in (b) are respectively the shock and post-shock temperatures obtained using the treatment of Foltz and Grace (1969).

Figure 11. Comparison of observed and calculated temperatures in quartz. In (a) the dashed line and solid line are the values of Wackerle (1962), corrected for T = 24°C. Asterisks (*) indicate residual temperatures determined from the plotted Hugoniot temperatures using estimated release volumes. In (b) the dashed lines are Hugoniot temperatures calculated as per Ahrens et al. (1969) for Hugoniot elastic limits as indicated; the solid line is the release temperature for an H.E.L. of 6 GPa. The heavy solid line shows the values of Mashimo et al. (1978).

Figure 12. Observed and calculated temperatures for Bamble bronzite. Solid curves are post-shock temperatures, broken curves Hugoniot temperatures.

(a) A, A': theoretical Hugoniot γ = .907

B, B': theoretical Hugoniot, γ = 2.5 on compression, 1 on release

C, C': actual Hugoniot, γ = .907, Hugoniot elastic limit of 6.7 GPa (Ahrens and Gaffney, 1971).

(b) D, D': theoretical Hugoniot, $\gamma = 1.57$

E, E': actual Hugoniot, $\gamma = 1.57$, Hugoniot elastic limit of 6.7 GPa

Figure 13. Observed and theoretical temperatures for forsterite

(a) A, A': polycrystalline forsterite, equilibrium Hugoniot

B, B': $\sim$ 4% porous forsterite, equilibrium Hugoniot

C, C': theoretical Hugoniot

(b) D, D': theoretical Hugoniot, $\gamma = 2.5$ on compression, $\gamma = 1$ on release

E, E': actual Hugoniot, assumed Hugoniot elastic limit 5 GPa

F : actual Hugoniot elastic limit 9 GPa shock temperatures

Note: The measured H.E.L. was 8.7 GPa.

Figure 14. Schematic diagram illustrating elasto-plastic release path.

Figure 15. Two release paths having the same initial slope and area underneath yet different final volumes.

Figure B-1 Static and dynamic streak images produced upon shock compression of c-cut single crystal forsterite to 17 GPa. (a) Static image as seen through streak camera. (b) Streak image demonstrating two-wave shock structure recorded by inclined mirror. The angle γ, is related to the value of the Hugoniot elastic limit, see e.g. Ahrens et al. (1968).

Figure B-2 Shock pressure versus density plot for forsterite showing the position of the Hugoniot elastic limit. The isentropic compression curve was calculated using a value of the bulk modulus and its pressure derivative of 128.8 GPa and 5.37 (see Table 9).

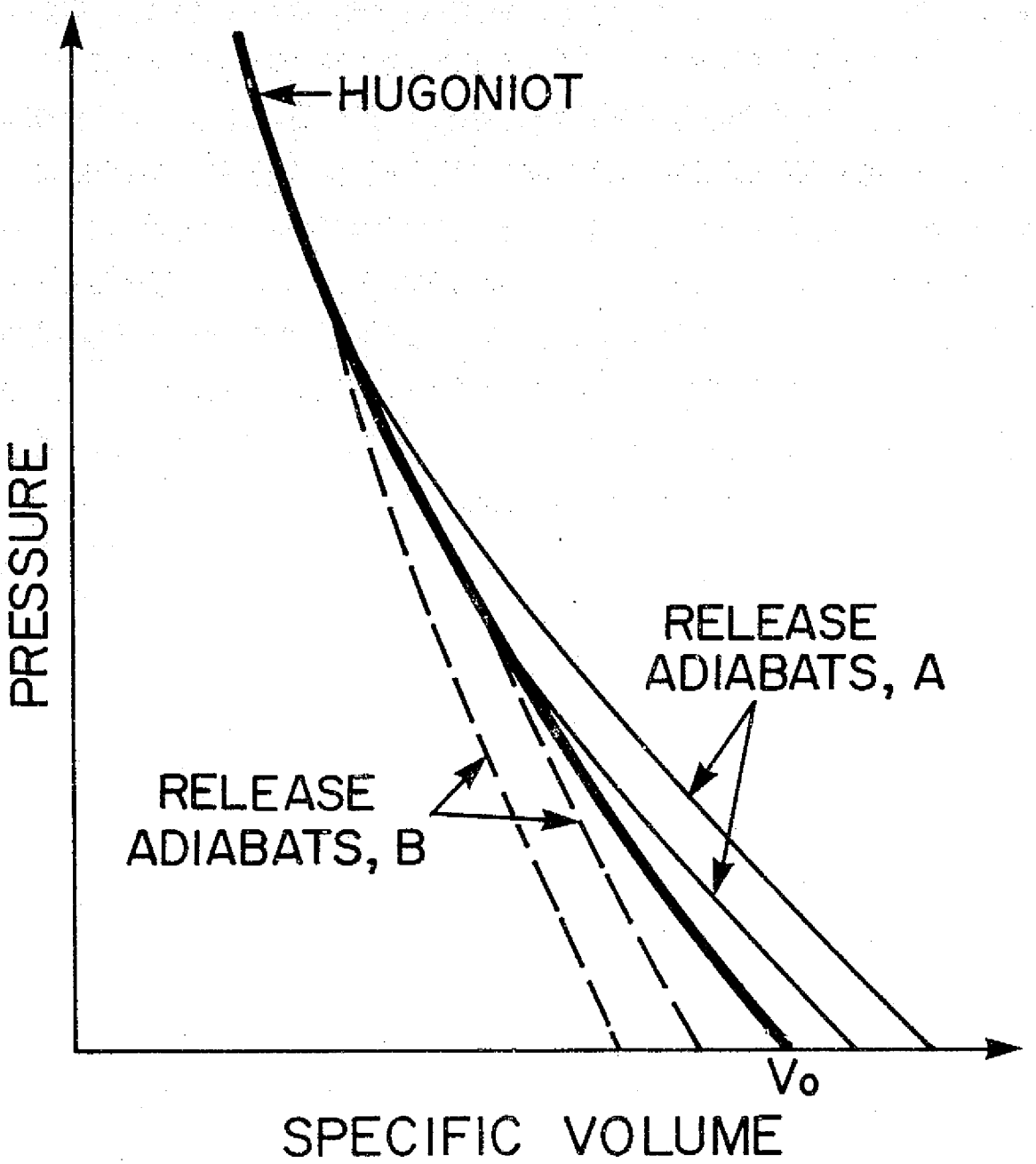
HUGONIOT
PRESSURE
RELEASE
ADIABATS, A
RELEASE
ADIABATS, B
Vo
SPECIFIC VOLUME

Fig. 1

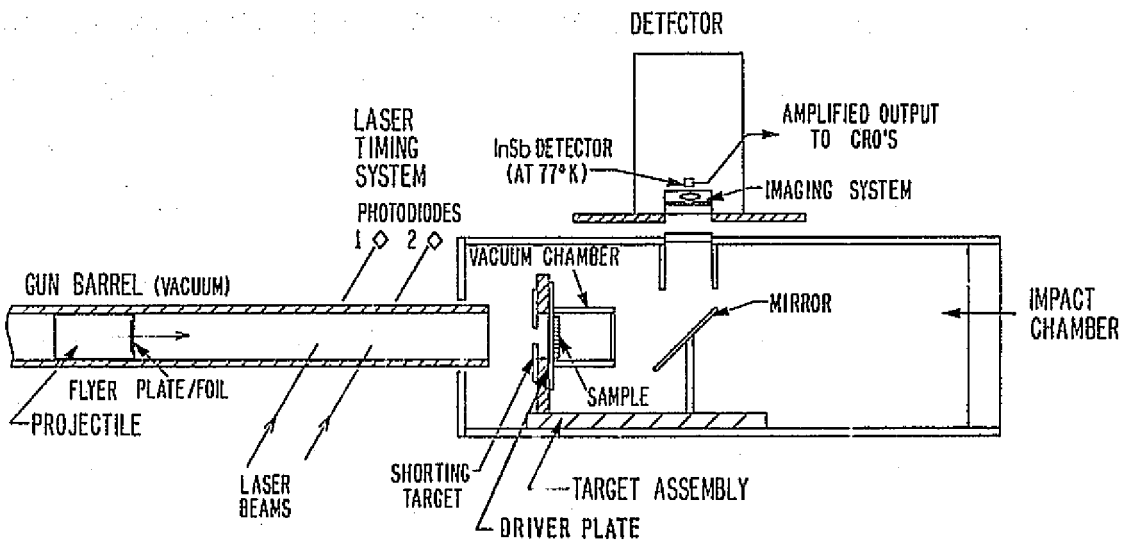
DETECTOR
LASER
TIMING
SYSTEM
InSb DETECTOR
(AT 77°K)
AMPLIFIED OUTPUT
TO CRO'S
IMAGING SYSTEM
PHOTODIODES
1 2
VACUUM CHAMBER
GUN BARREL (VACUUM)
MIRROR
IMPACT
CHAMBER
FLYER PLATE/FOIL
PROJECTILE
SAMPLE
LASER
BEAMS
SHORTING
TARGET
TARGET ASSEMBLY
DRIVER PLATE

Fig. 2

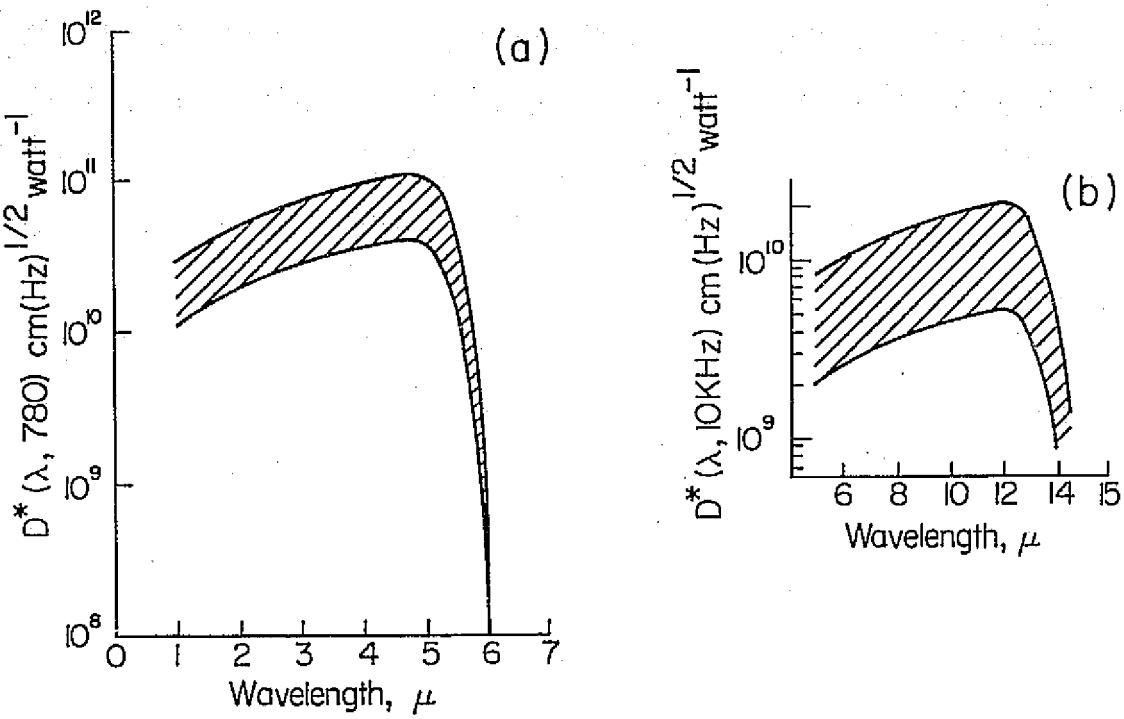
(a)
10^{12}
10^{11}
10^{10}
10^{9}
10^{8}
$D^*(\lambda, 780)$ cm(Hz)$^{1/2}$watt^{-1}
0 1 2 3 4 5 6 7
Wavelength, μ
(b)
10^{10}
10^{9}
$D^*(\lambda, 10KHz)$ cm(Hz)$^{1/2}$watt^{-1}
6 8 10 12 14 15
Wavelength, μ

Fig. 3

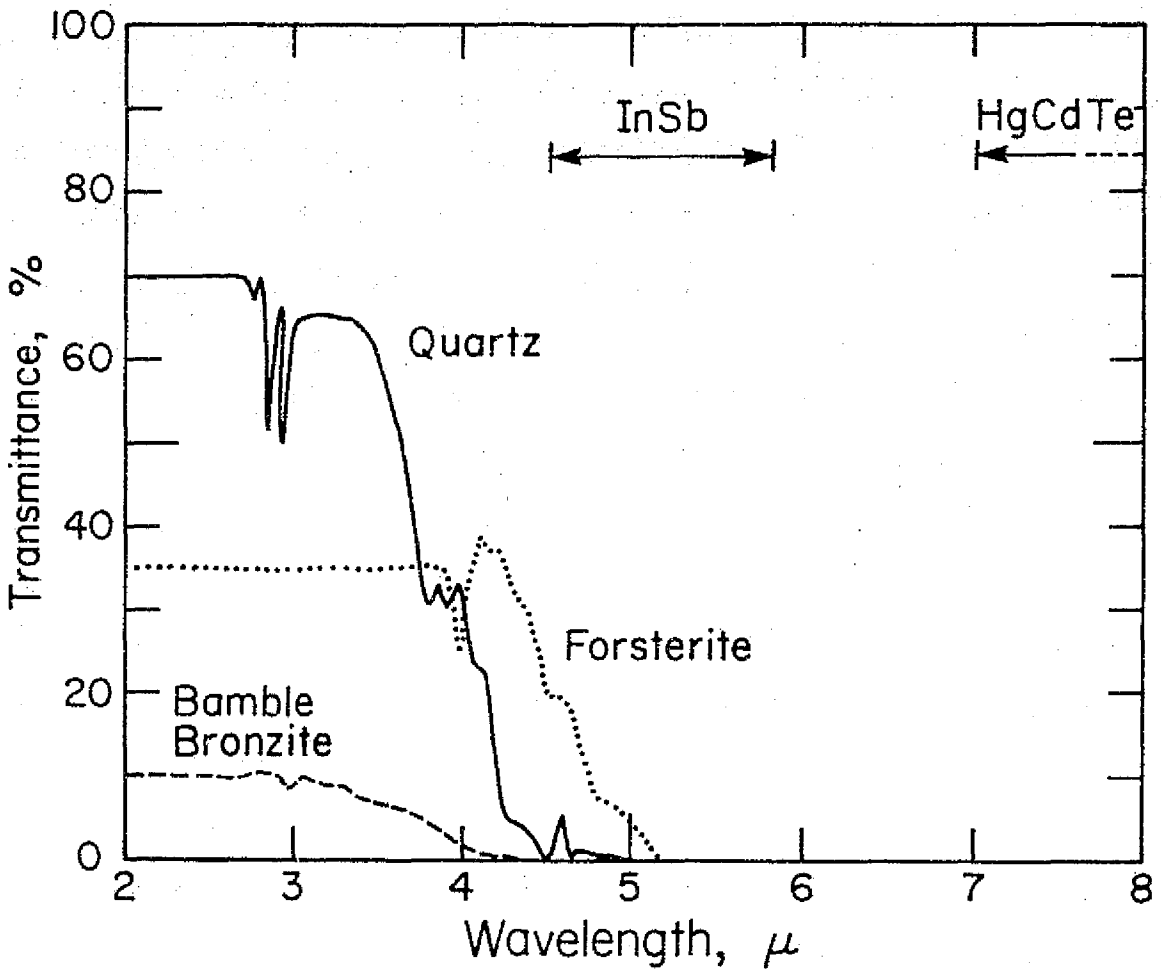
100
80
60
40
20
0
Transmittance, %
InSb
HgCdTe
Quartz
Forsterite
Bamble
Bronzite
2
3
4
5
6
7
8
Wavelength, μ

Fig. 4

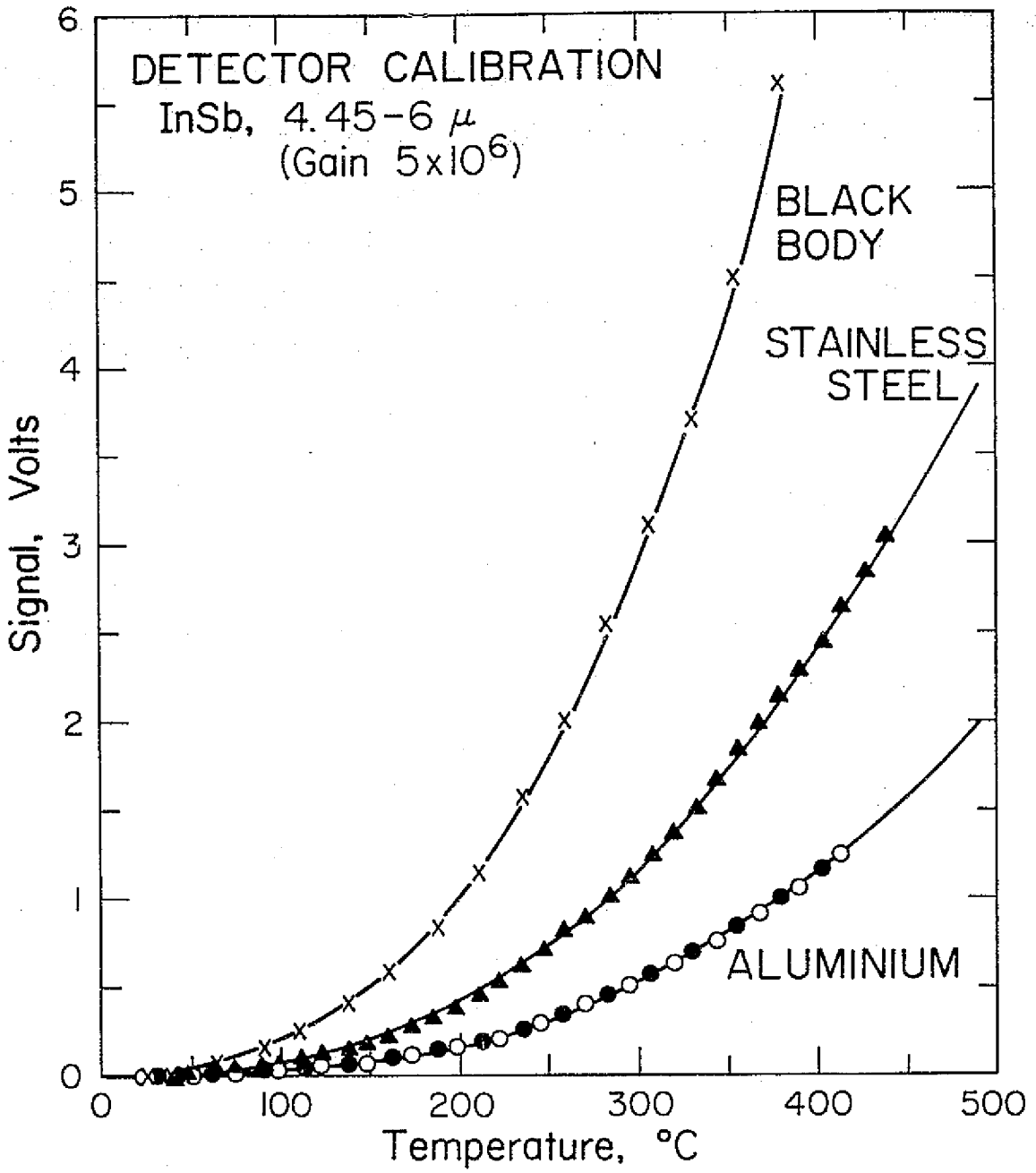
DETECTOR CALIBRATION
InSb, 4.45-6 μ
(Gain 5x10^6)
BLACK BODY
STAINLESS STEEL
ALUMINIUM
Signal, Volts
Temperature, °C
0
1
2
3
4
5
6
0
100
200
300
400
500

Fig. 5

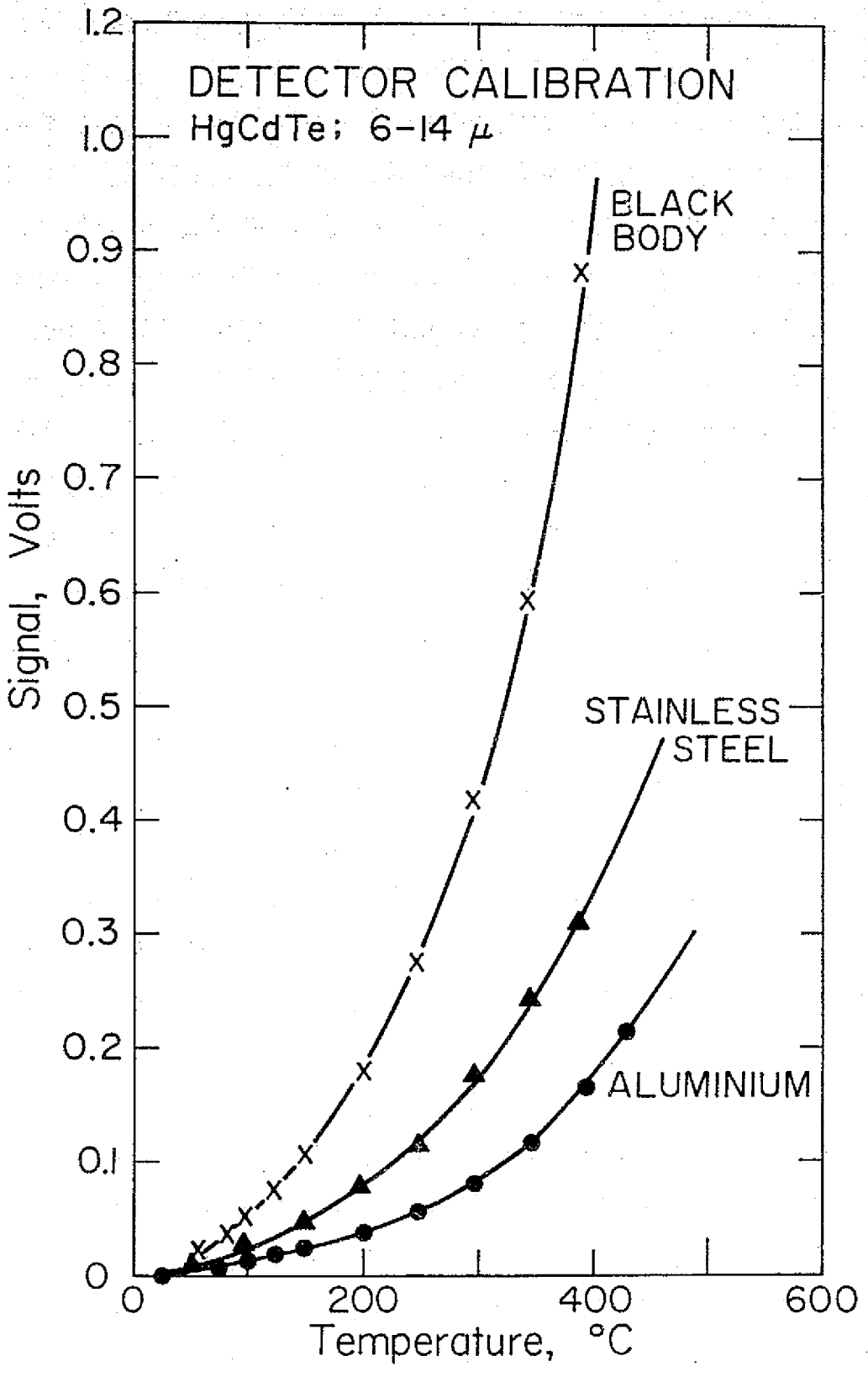
DETECTOR CALIBRATION
HgCdTe; 6-14 μ
BLACK BODY
STAINLESS STEEL
ALUMINIUM
Signal, Volts
Temperature, °C
1.2
1.0
0.9
0.8
0.7
0.6
0.5
0.4
0.3
0.2
0.1
0
0
200
400
600

Fig. 6

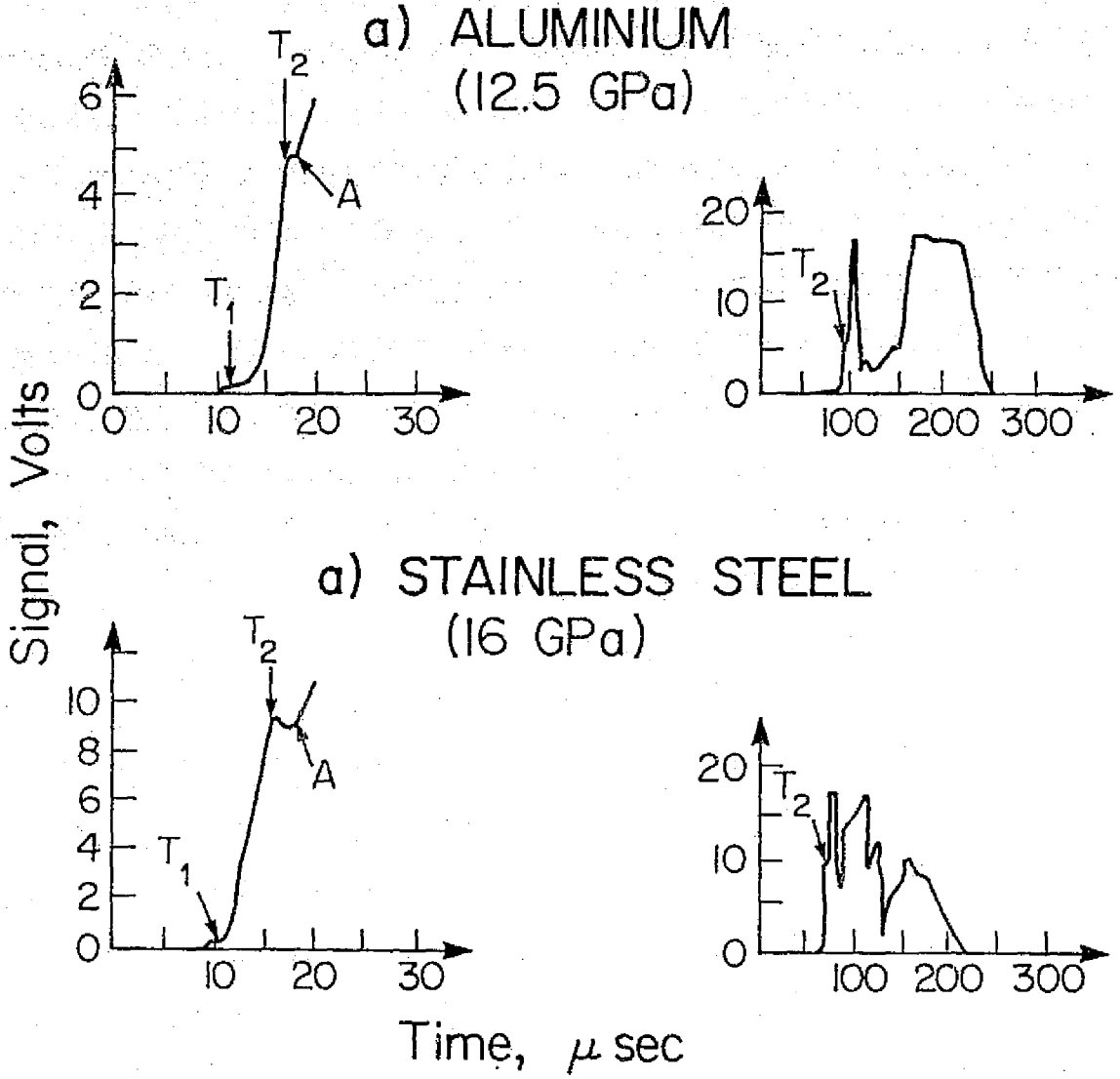
a) ALUMINIUM
(12.5 GPa)
a) STAINLESS STEEL
(16 GPa)
Signal, Volts
Time, μ sec
T1
T2
A
0
2
4
6
10
20
30
100
200
300
8

Fig. 7

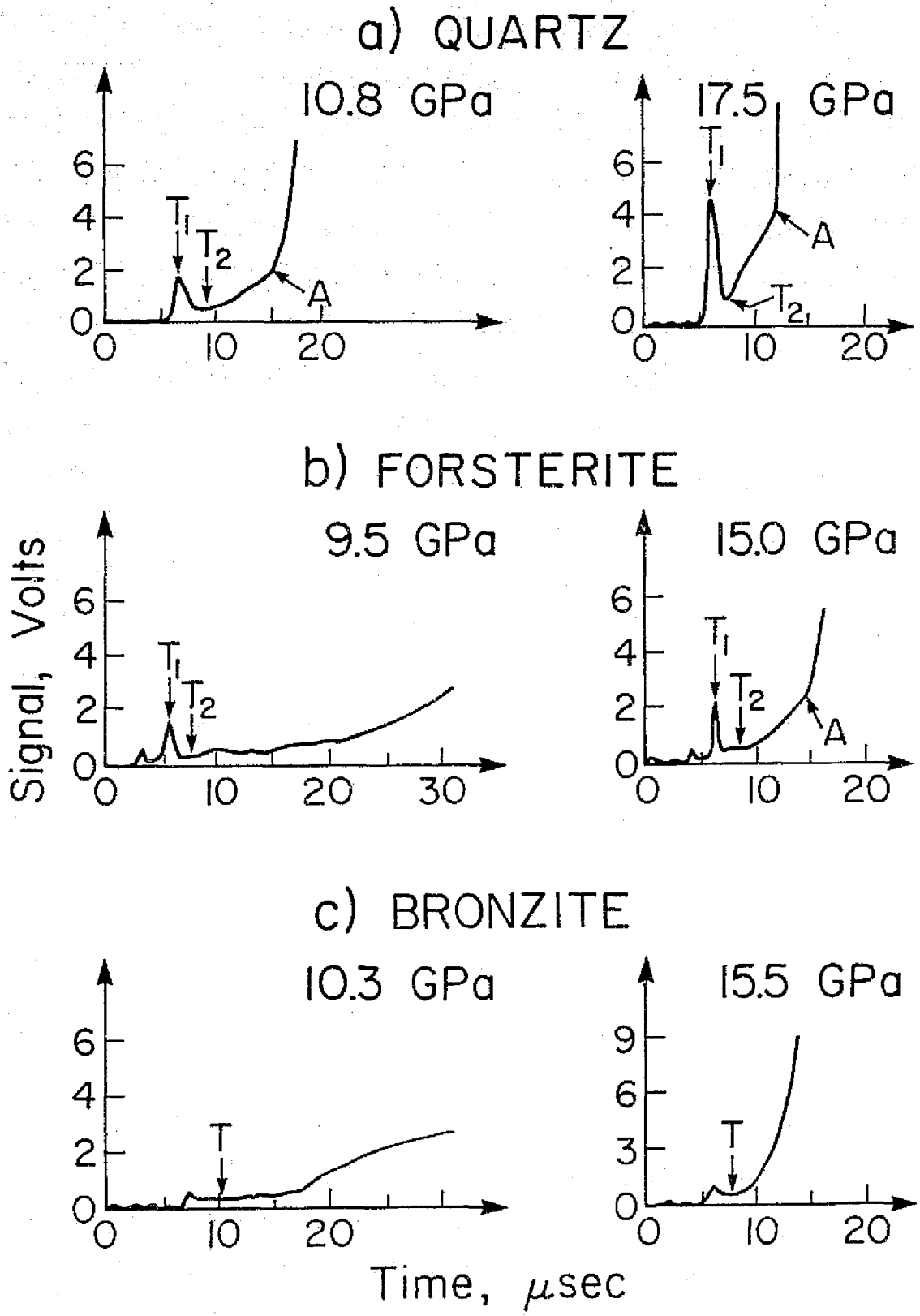
a) QUARTZ
10.8 GPa
17.5 GPa
b) FORSTERITE
9.5 GPa
15.0 GPa
c) BRONZITE
10.3 GPa
15.5 GPa
Signal, Volts
Time, μsec
T1
T2
A
T

Fig. 8

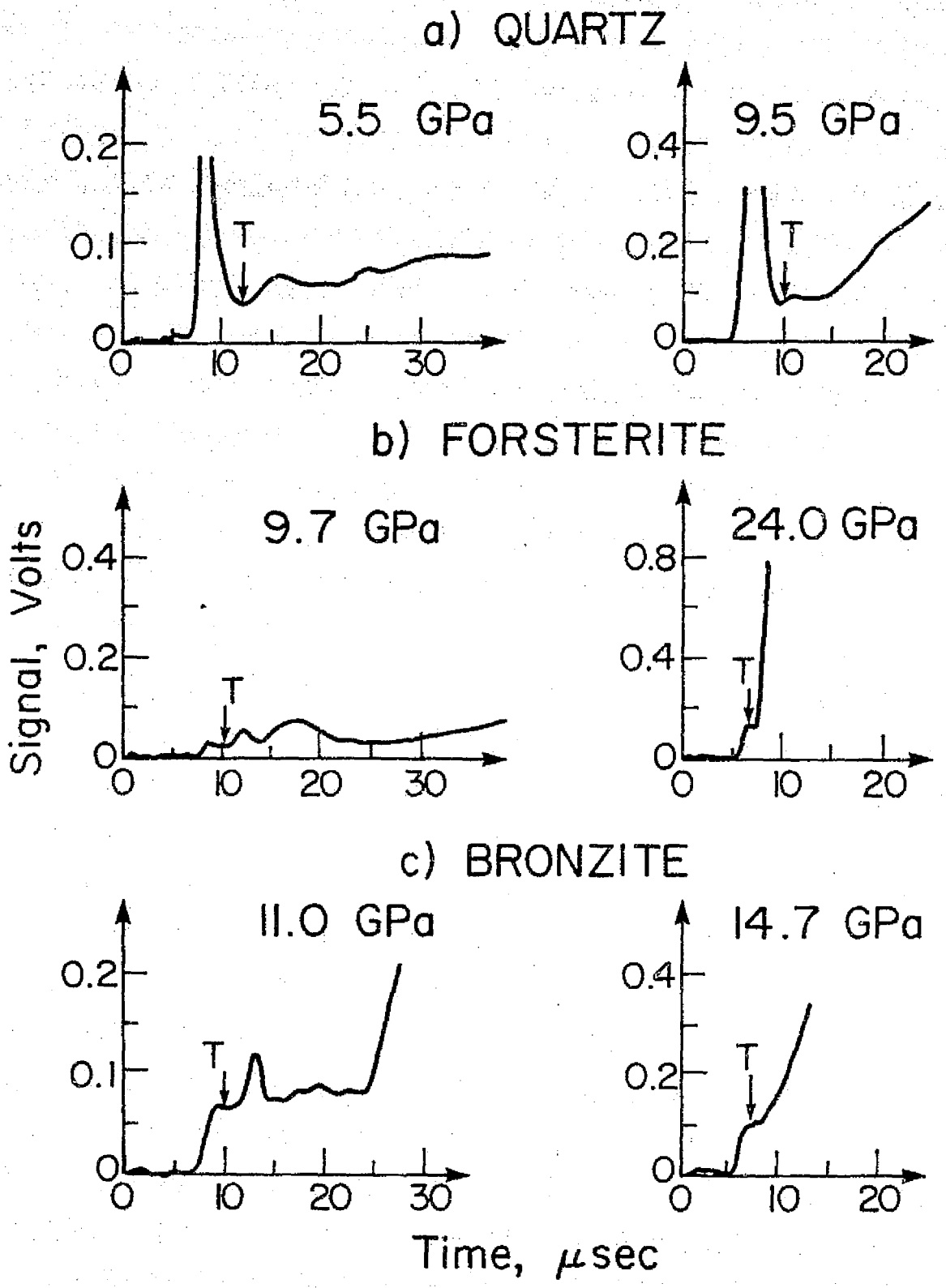
a) QUARTZ
5.5 GPa
9.5 GPa
b) FORSTERITE
9.7 GPa
24.0 GPa
c) BRONZITE
11.0 GPa
14.7 GPa
T
Signal, Volts
Time, μsec

Fig. 9

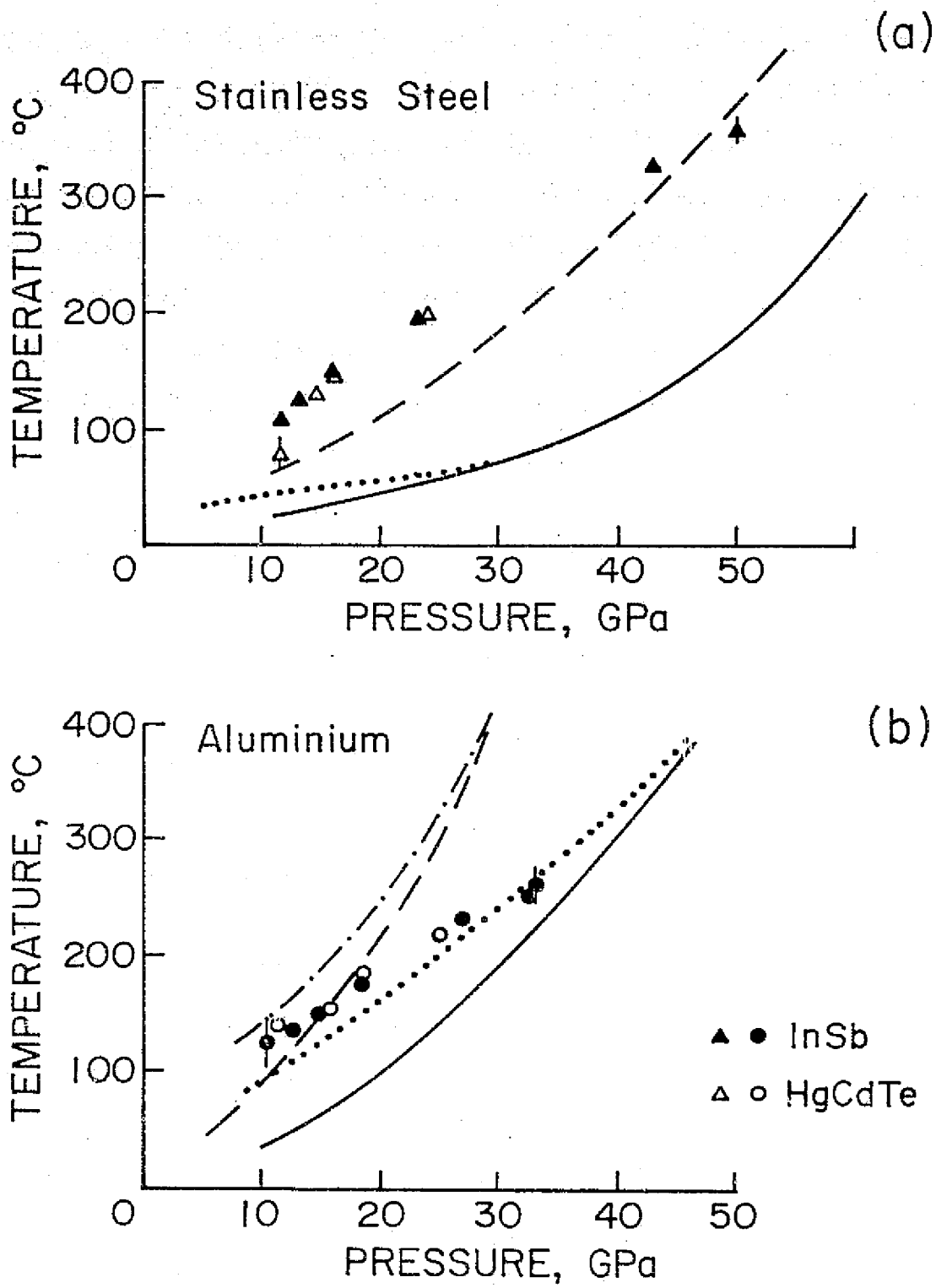
(a)
Stainless Steel
TEMPERATURE, °C
400
300
200
100
0
10
20
30
40
50
PRESSURE, GPa
(b)
Aluminium
TEMPERATURE, °C
400
300
200
100
0
10
20
30
40
50
PRESSURE, GPa
▲ ● InSb
△ ○ HgCdTe

Fig. 10

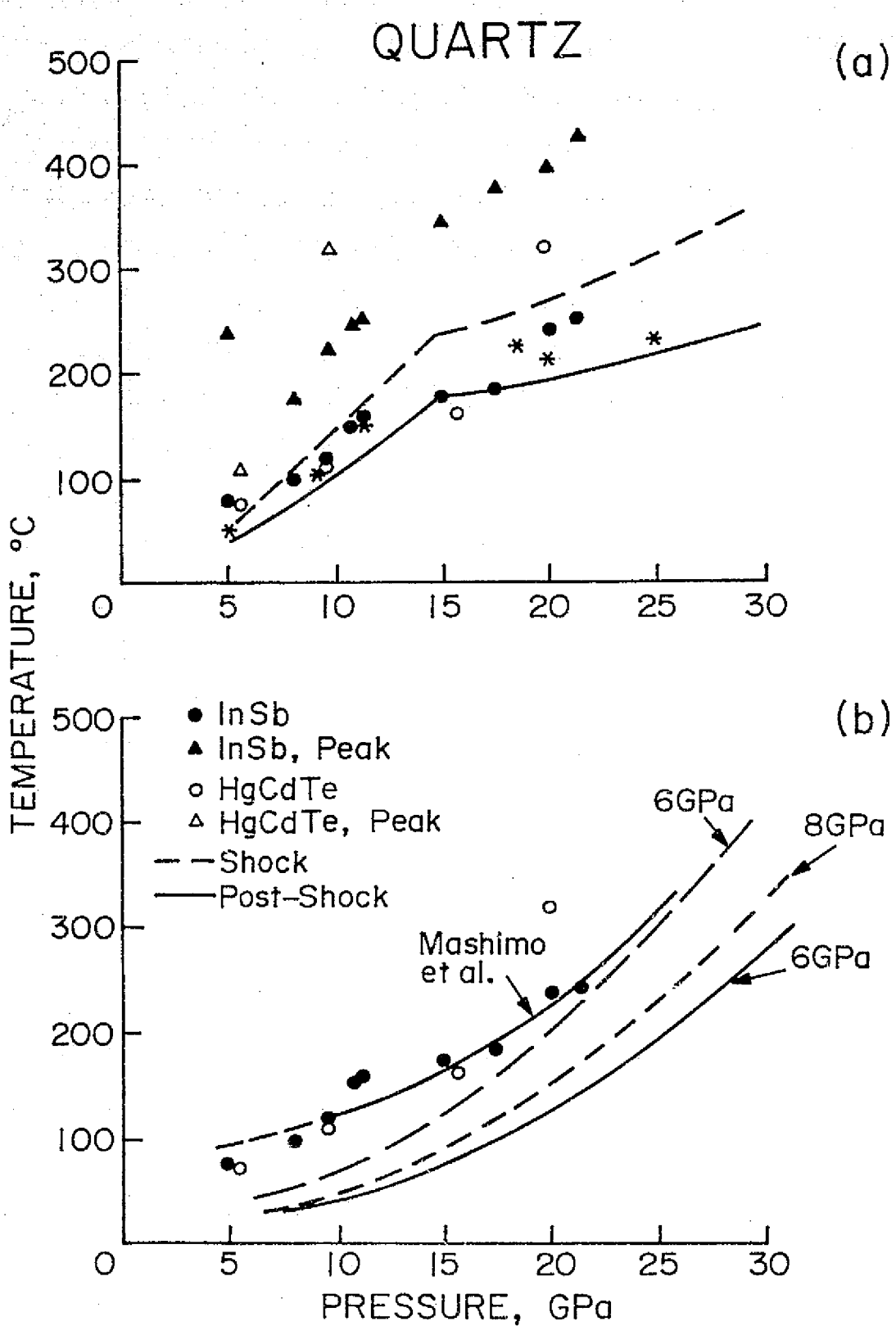
QUARTZ
(a)
500
400
300
200
100
0
5
10
15
20
25
30
TEMPERATURE, °C
(b)
InSb
InSb, Peak
HgCdTe
HgCdTe, Peak
Shock
Post-Shock
6GPa
8GPa
6GPa
Mashimo
et al.
PRESSURE, GPa

Fig. 11

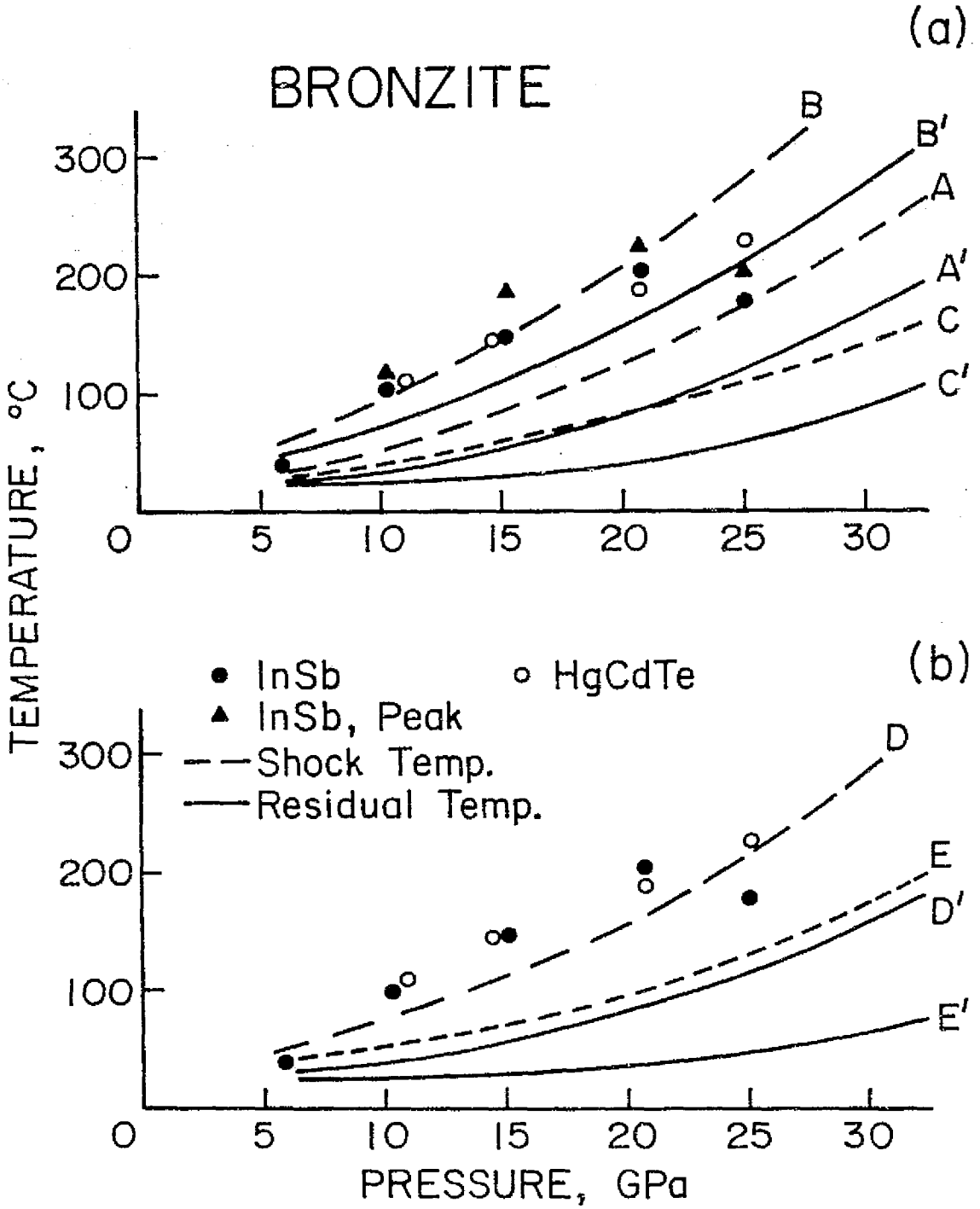
(a)
BRONZITE
B
B'
A
A'
C
C'
300
200
100
0
5
10
15
20
25
30
TEMPERATURE, °C
(b)
● InSb
○ HgCdTe
▲ InSb, Peak
– – Shock Temp.
—— Residual Temp.
D
E
D'
E'
PRESSURE, GPa

Fig. 12

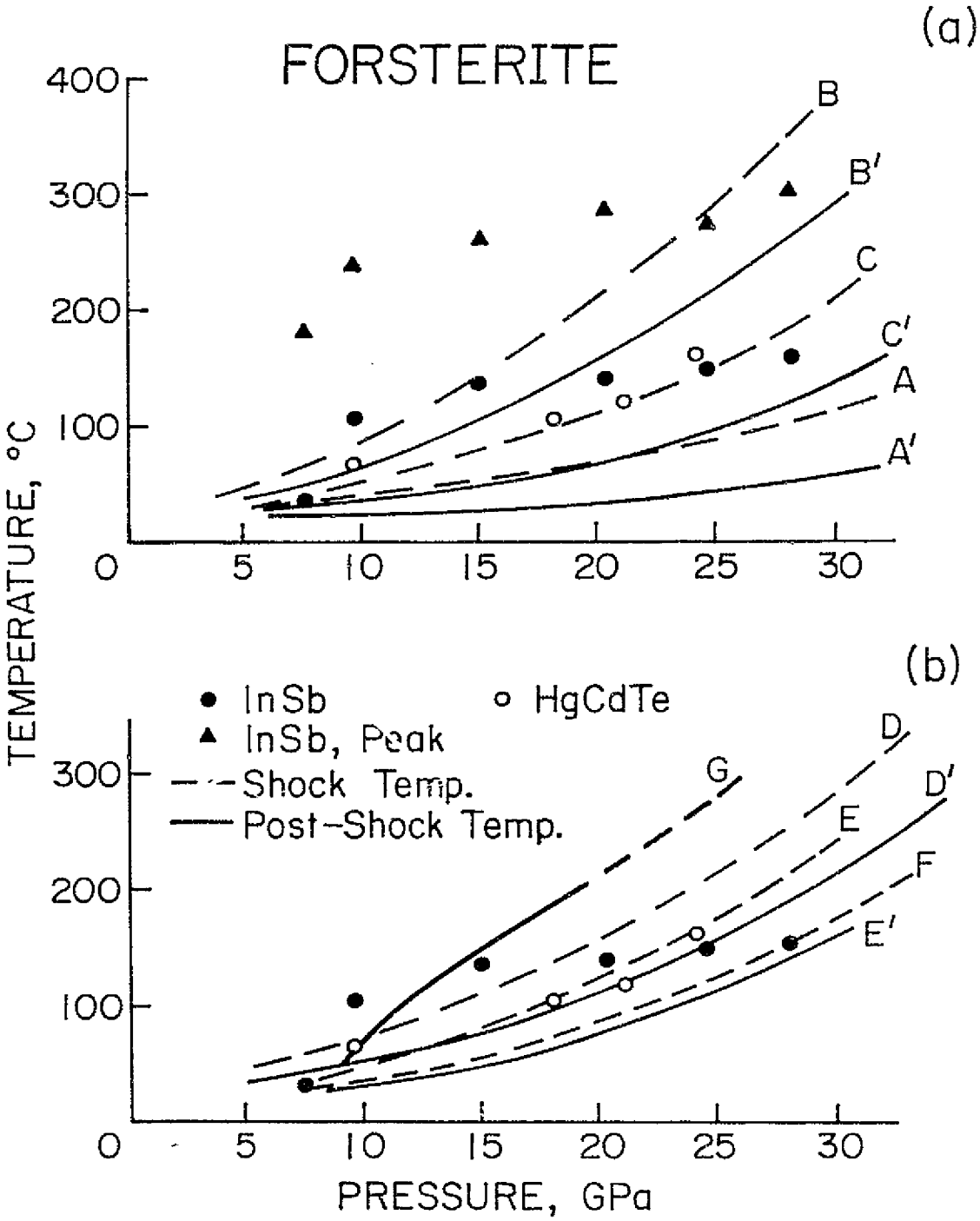
(a)
FORSTERITE
400
300
200
100
0
B
B'
C
C'
A
A'
5
10
15
20
25
30
(b)
InSb
HgCdTe
InSb, Peak
Shock Temp.
Post-Shock Temp.
D
D'
G
E
F
E'
300
200
100
0
5
10
15
20
25
30
TEMPERATURE, °C
PRESSURE, GPa

Fig. 13

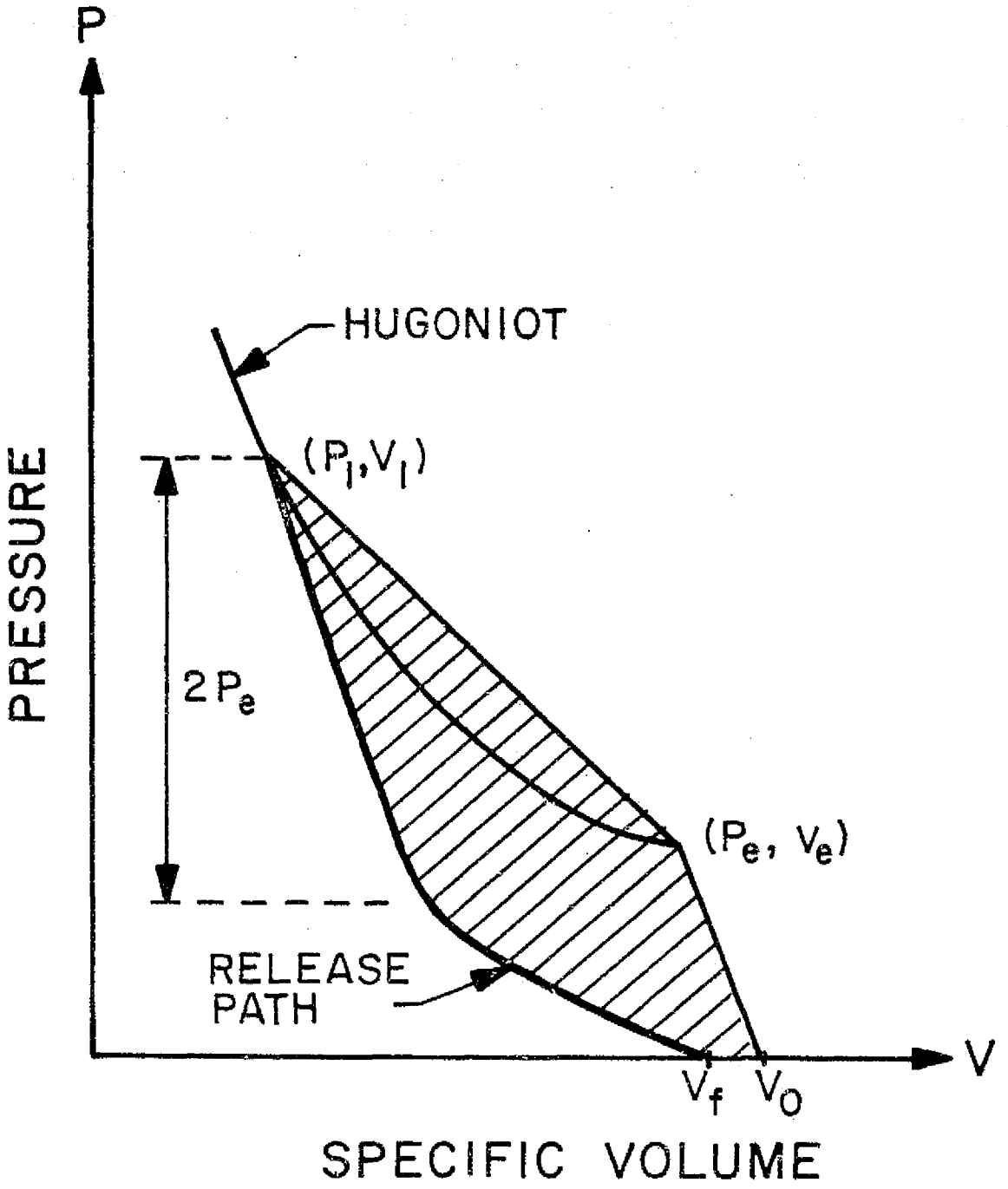
P
PRESSURE
HUGONIOT
(P_1, V_1)
$2P_e$
(P_e, V_e)
RELEASE
PATH
V
V_f
V_0
SPECIFIC VOLUME

Fig. 14

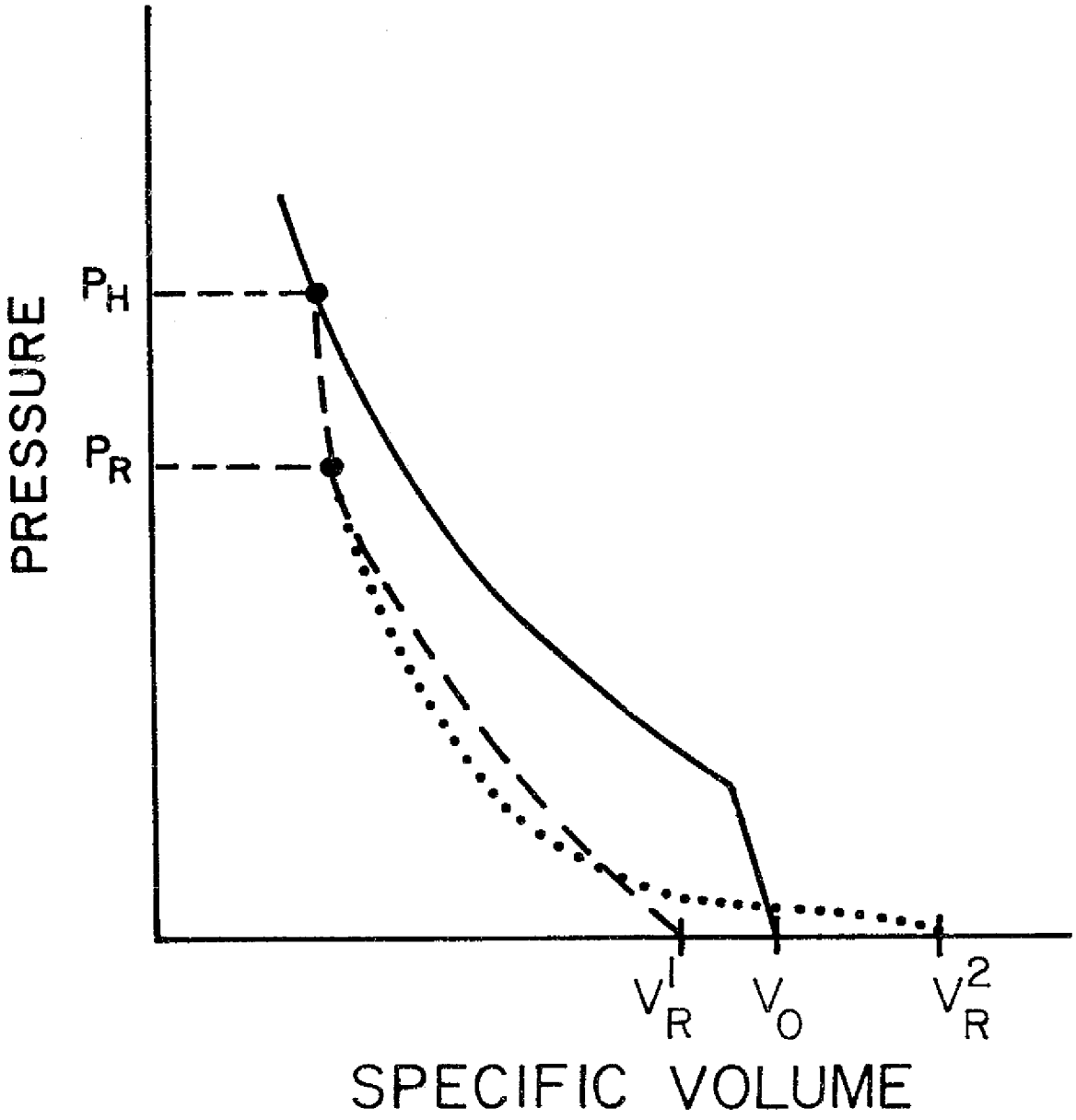

Fig. 15

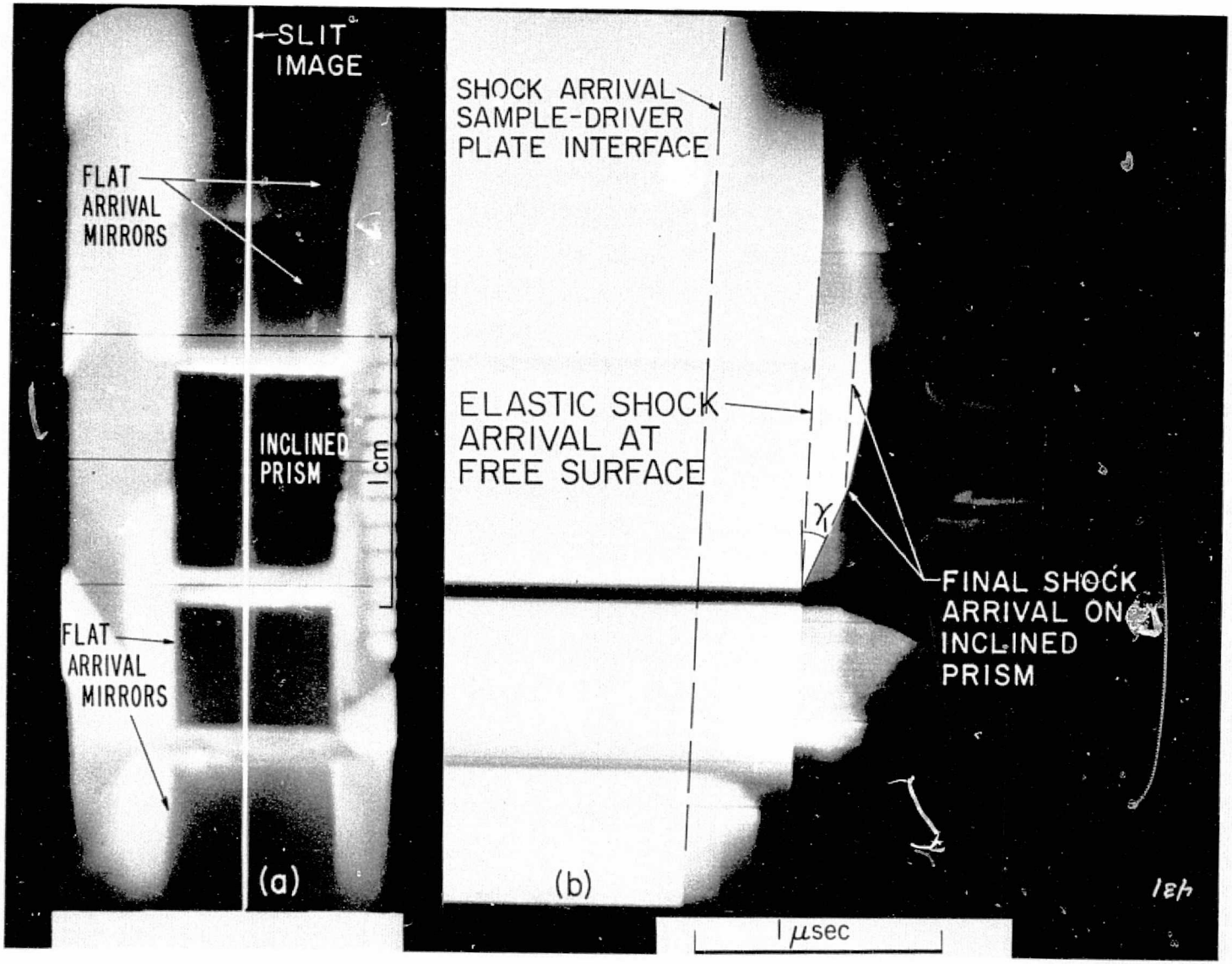

Fig. B-1

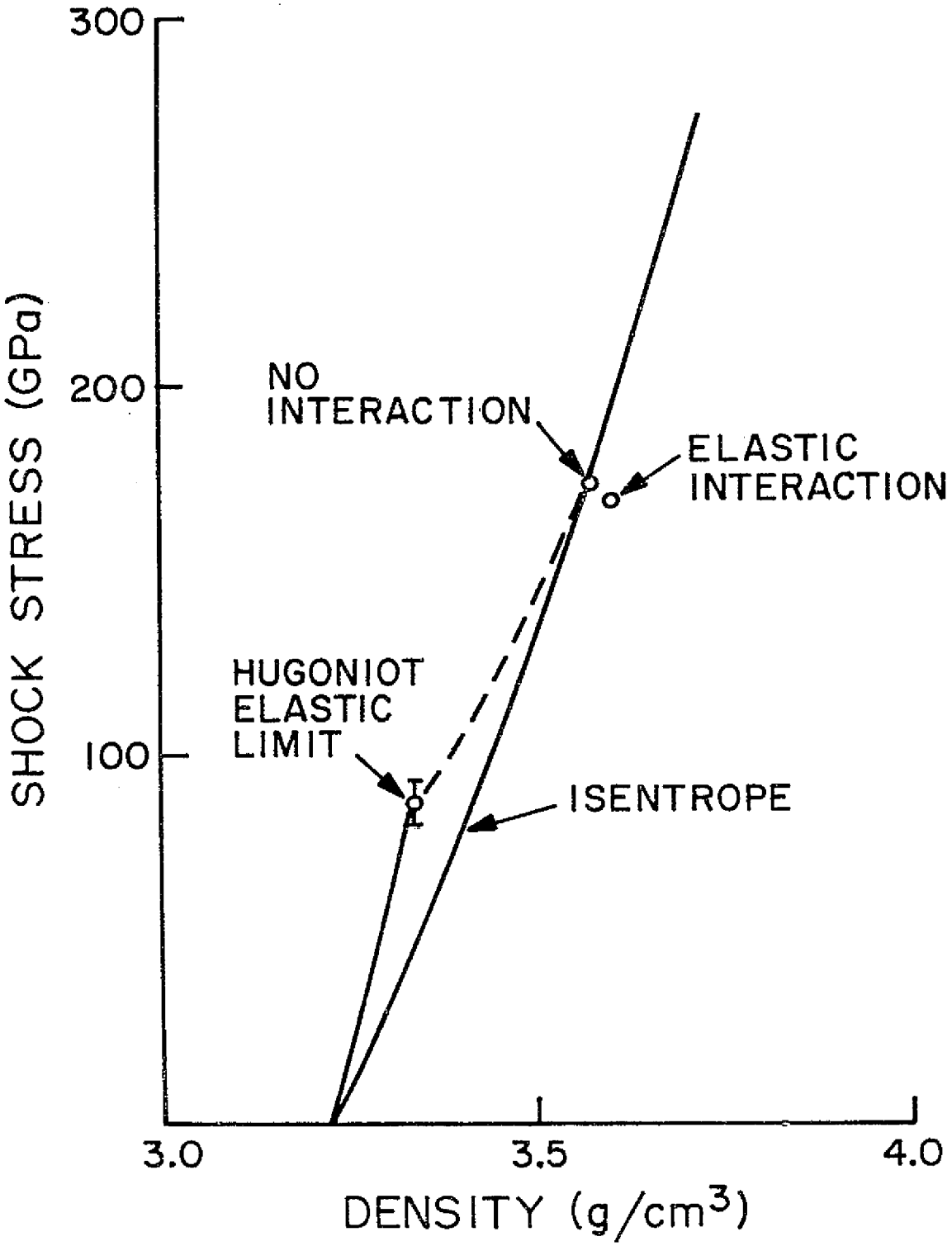
300
200
100
SHOCK STRESS (GPa)
NO
INTERACTION
ELASTIC
INTERACTION
HUGONIOT
ELASTIC
LIMIT
ISENTROPE
3.0
3.5
4.0
DENSITY (g/cm3)

Fig. B-2